Lithographic Imaging Techniques for the Formation of Nanoscopic Features

G. M. Wallraff* and W. D. Hinsberg

IBM Almaden Research Center, 650 Harry Road, San Jose, California 95120-6099

Received October 20, 1998 (Revised Manuscript Received April 21, 1999)

Contents

I.	Overview	1801
II.	Introduction	1801
III.	Background	1802
	A. Lithography	1802
	B. Photoresist Technology	1803
	C. Roadmap to Nanometer Sized Devices	1809
IV.	Imaging Technologies	1809
	A. Next-Generation Optical Lithography	1809
	B. Particle Beams	1813
	C. EUV	1815
	D. Proximity X-ray	1816
V.	High-Resolution Resists	1818
	A. Latent Image Formation	1818
	B. Line-Edge Roughness	1819
VI.	Summary	1820
VII.	References	1820

I. Overview

Over the past 30 years the world market for semiconductors has grown at an average annual rate of approximately 15%. This growth has been maintained by the industry's unique ability to consistently provide over this time frame higher device performance at lower cost (achieving a 25−30% per-year cost reduction per function). Microlithography is the key technological driving force for this; in large part, the overall rate of progress in microelectronics is controlled by the rate of advances in microlithographic tools, methods, and materials. Today, the photolithographic technologies that have served the microelectronics community since its inception are widely viewed to be nearing their limits of extendibility. If the historical growth rate is to be maintained in the future, new imaging technologies with the capability of forming features with sub-100 nm dimensions must be devised and refined. In this paper we provide an overview of the issues to be considered for patterning in the sub-100 nm regime and describe the imaging technologies which are currently being evaluated for such use.

II. Introduction

It will be of immense practical value if current research in nanofabrication ultimately defines a set of tools and methods that provide capability for the construction of structures of arbitrary shape, formed with high precision from a wide range of materials, at low cost and high speed, where the smallest feature is less than 0.001 μm^3 in volume. At the current state of the art, however, no one approach exists that can simultaneously meet all these criteria.

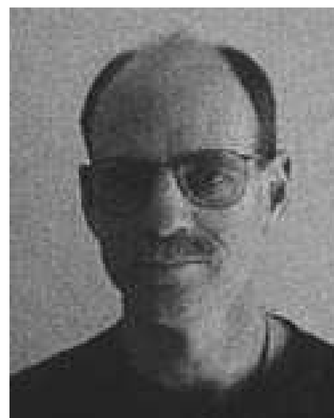

Gregory Wallraff received his Ph.D. from the University of Utah. He joined the Optical Lithography Group at the IBM Almaden Research Center in 1987. He is currently working on developing new materials for next-generation lithographic applications.

William Hinsberg was trained in Chemistry at the University of Michigan, Caltech, and Stanford University. He joined IBM in 1982, where he has carried out research in several areas, with a focus on lithographic materials and processing. Currently, he also is a Senior Investigator in the Center on Polymer Interfaces and Macromolecular Assemblies (CPIMA), an NSF-funded Material Science Research and Engineering Center.

In self-assembly methods, kinetic and thermodynamic properties of the system control the formation of highly ordered two- and three-dimensional structures. Nanostructures constructed by self-assembly (i.e., carbon nanotubes,[1] polymer dendrimers,[2] and semiconductor clusters[3]) are not fabricated as much as they are grown. One strength of self-assembly is

10.1021/cr980003i CCC: $35.00 © 1999 American Chemical Society
Published on Web 06/25/1999

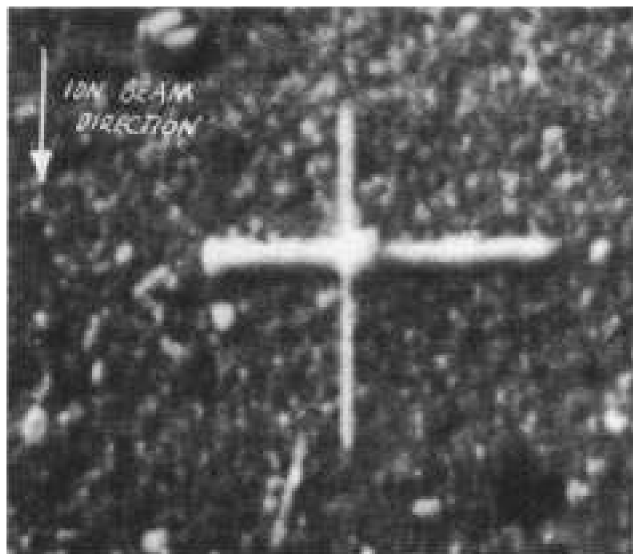

Figure 1. Scanning electron micrograph of a copper pattern formed by electron-beam lithography followed by image transfer using ion-beam etching. This structure, fabricated in 1964, was an early demonstration of the capabilities of nanolithography (Reprinted with permission from ref 5. Copyright 1964 Wiley and Sons.)

that its inherent parallelism allows a vast quantity of structures to be fashioned rapidly and in an economical manner. However, the size and shape of such a structure is determined by the chemical and physical forces that direct its formation rather than by the requirements of its end application. This greatly restricts the broad utility of such an approach.

The ultimate in control is achieved when a structure can be assembled atom by atom. This has been demonstrated by the manipulation of atoms and molecules using the tip of a scanning tunneling microscope (STM).[4] To date, this approach is specific to few substances and substrates and, since the structures are built one at a time, is not capable of high throughput.

It is worthwhile to keep in mind that the routine ability to generate structures of arbitrary shape on the nanometer scale has been available for well over 3 decades.[5] Figure 1 depicts an example of a sub-100 nm feature produced with a modified scanning electron microscope in an early demonstration of the potential of microlithography. Today microphotolithographic technology is used daily to produce uncounted trillions of structures with printed feature dimensions of 250 nm (the final device dimensions can be as small as 120−150 nm). In less than 10 years, high-volume manufacturing of integrated circuits with dimensions of 70 nm is projected to begin[6] (see Figure 2).

The establishment of an economical technology for high-volume manufacturing at these very small feature sizes is the daunting challenge facing the semiconductor industry. In the following report, we summarize the imaging technologies that are currently being developed to address this challenge. Recently, nonlithographic techniques have been developed for use in fabricating submicron sized features. These approaches are described elsewhere.[7]

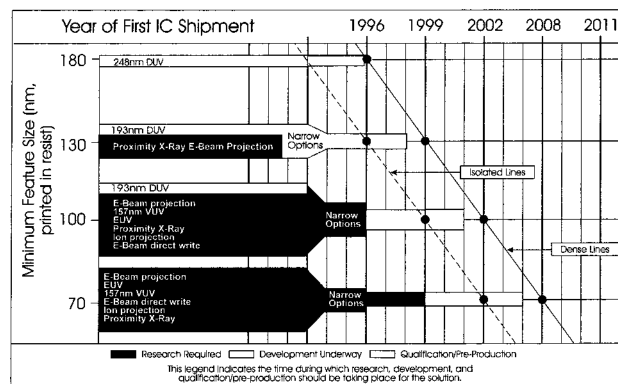

Figure 2. Projected semiconductor feature sizes and proposed year of implementation. The proposed lithographic solutions for each generation are included. This is a revised version of the 1997 SIA Roadmap. (Reprinted with permission of International SEMATECH.)

III. Background

A. Lithography

In its original meaning, the term lithography refers to a process of printing using a nonpolar ink applied to a hydrophilic master plate patterned with a hydrophobic image.[8] In its current modern usage, the term is more generally applied to a number of methods for replicating a predetermined master pattern on a substrate. Most commonly, replication is effected by first coating the substrate with a radiation-sensitive polymer film (a resist) and then exposing the film to actinic radiation in a patternwise manner. The radiation chemistry that results alters the physical or chemical properties of the exposed areas of the film such that they can be differentiated in a subsequent image development step. Most commonly, the solubility of the film is modified with the radiation chemistry either increasing the solubility of exposed areas (yielding a positive image of the mask after develop) or decreasing the solubility to yield a negative-tone image of the mask. Figure 3 displays a schematic of the overall imaging process.

While X-radiation or high-energy electron beams are used for certain specialized applications, by far most microdevices today are fabricated using optical projection photolithography. In this technique the image of light transmitted through a mask is precisely focused onto a resist-coated wafer using a complex system of lenses (Figure 4).

The minimum resolution R achievable with projection lithography is governed by the relation

$$R = k_1\lambda/\mathrm{NA} \tag{1}$$

where λ is the wavelength of exposing radiation, k_1 is a process-dependent parameter in the range of 0.4−1, and NA is the numerical aperture, equal to the refractive index of the surrounding medium (~1 for air) times the sine of the angle subtended by the objective lens of the system.[10]

The depth of focus (DOF) for the same tool is given by the equation

$$\mathrm{DOF} = k_2\lambda/(\mathrm{NA})^2 \tag{2}$$

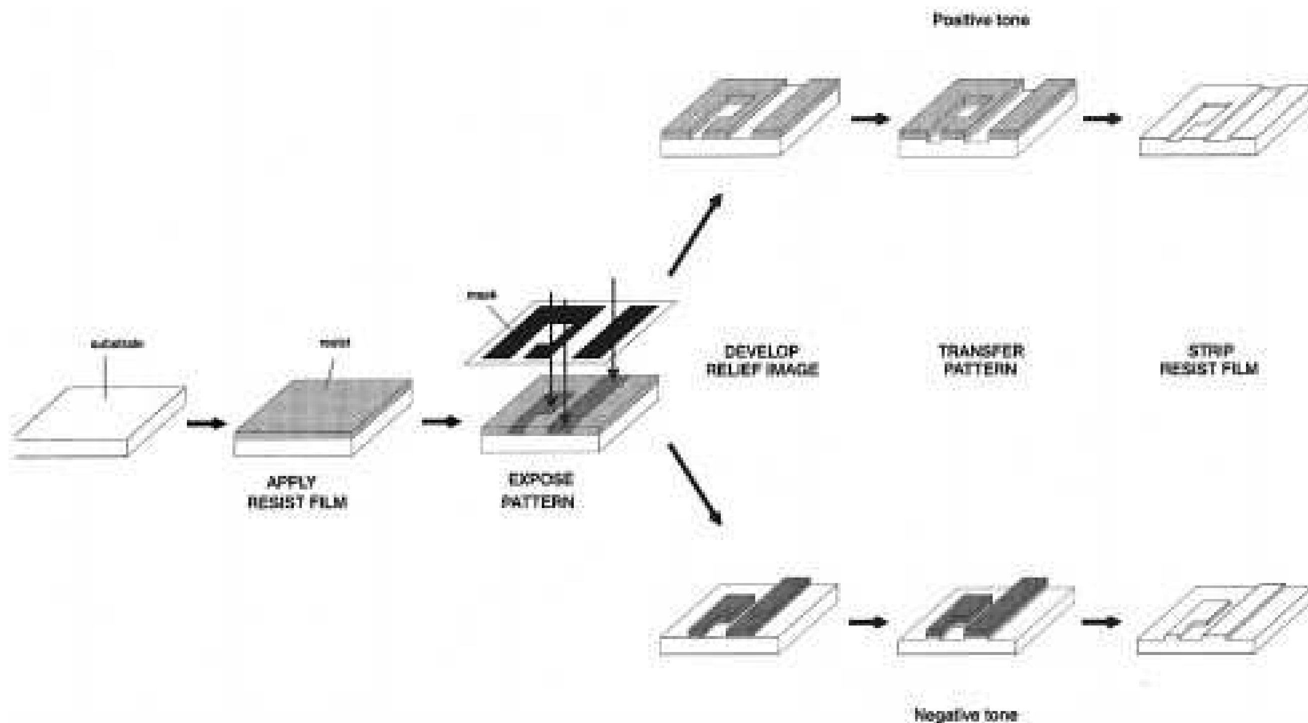

Figure 3. Schematic diagram of the lithographic process.

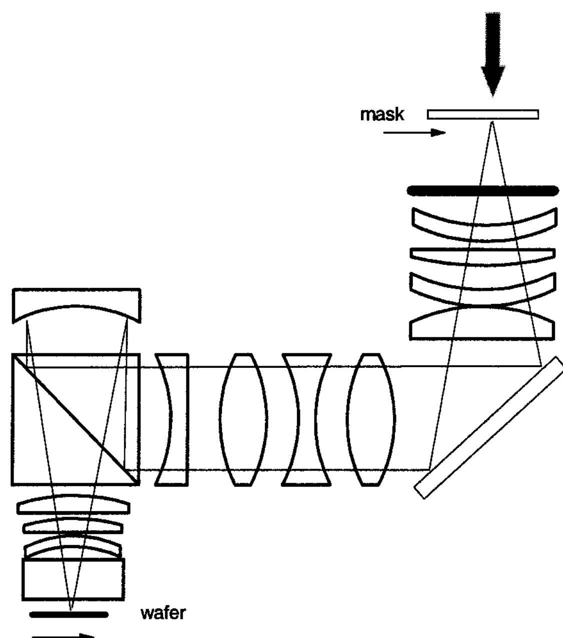

Figure 4. Schematic of representative projection optical system 248 nm DUV exposure tool (See ref 9). In this tool, only a portion of the mask is illuminated. The mask and wafer are scanned synchronously through the illuminating beam to expose the complete pattern.

where k_2 is a process-dependent parameter on the order of 0.5−1 and λ and NA are defined as before. A large value for DOF is desired as it increases the tolerance of the process to deviation of the substrate surface from perfect planarity.

The evolutionary refinement of projection optical lithography from its introduction can be understood by consideration of these equations. The overall goal is improved resolution while maintaining a maximum DOF. Resolution improvements may be realized by reducing the wavelength (λ) of actinic exposure either by increasing the NA or by process and tool refinements that reduce the value of k_1. There are practical limits to each of these approaches, however.

Improved resolution by increasing the NA of the lens system requires that either the diameter of the lens be increased or the focal length be reduced. The result is increased lens size and mass, along with increased complexity of the overall lens system to provide correction for optical aberrations. Since the NA appears as a squared term in the equation for DOF, a resolution improvement achieved via increased NA is accompanied by a proportionately larger decrease in DOF.

Improved resolution achieved by a reduction in the exposing wavelength does not incur as great a penalty in DOF but has the requirement that a suitable photoresist, light source, and selection of optical lens materials be available for the decreased wavelength. The development of new generations of photoresist for leading edge microlithography applications has been driven in large part by the need for imaging materials optimized for a specific exposure wavelength (Figure 2).

B. Photoresist Technology

DNQ−Novolak Photoresists. The bulk of the world's semiconductors are manufactured using diazonaphthoquinone (DNQ)-based photoresists and exposure tools equipped with mercury arc lamp illumination sources (producing UV wavelengths of 365 or 436 nm).[11] These photoresists evolved from materials first developed for the printing industry and consist of the photoactive DNQ dispersed in a phenolic matrix resin (a low molecular weight condensation product of formaldehyde and cresol isomers known as novolak). The hydrophobic diazonaphthoquinone acts as a dissolution inhibitor to retard the

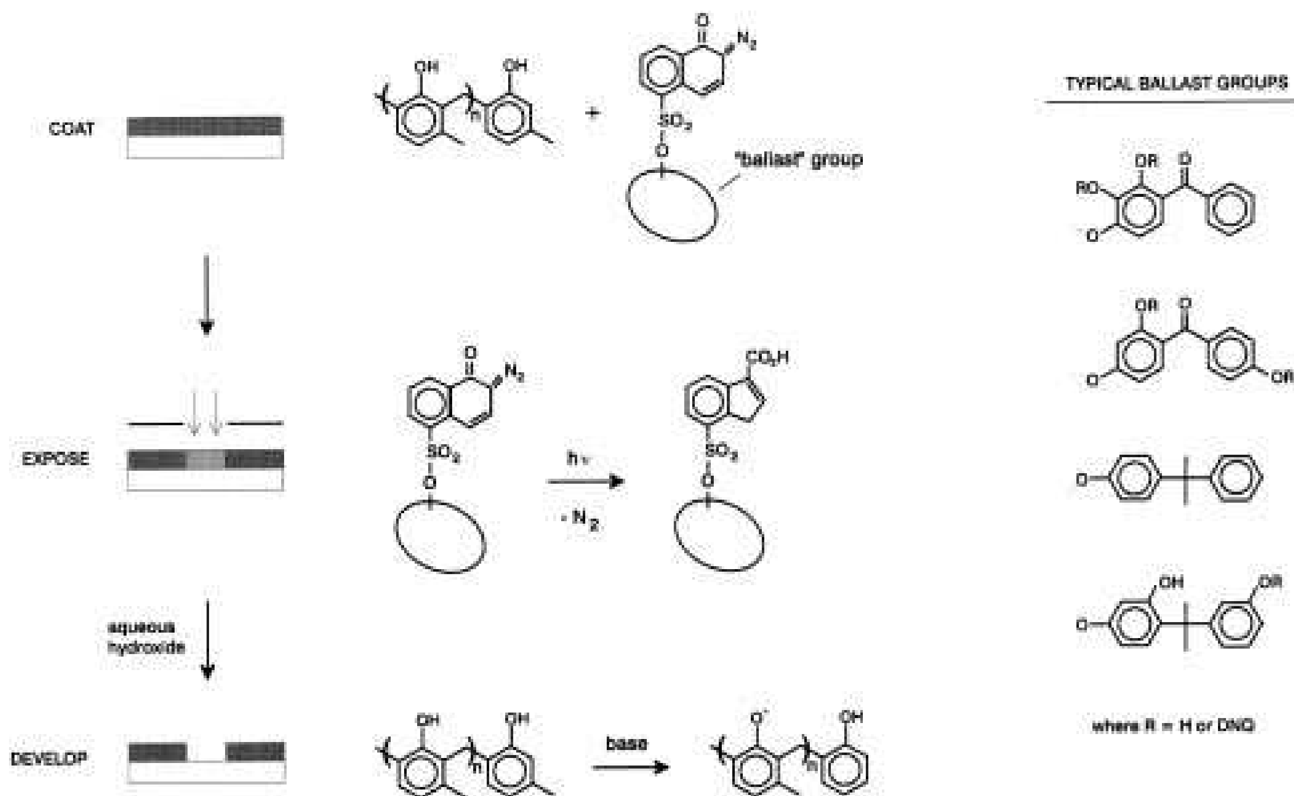

Figure 5. Imaging and development chemistry for DNQ-based photoresists.

dissolution of the weakly acidic polymer in the aqueous alkaline solutions used as the development medium. Irradiation of selected regions of this film (through the transparent regions of the mask in Figure 5) results in the transformation of the hydrophobic DNQ (via a photochemical Wolff rearrangement) into the hydrophilic indenecarboxylic acid (Figure 5). The exposed regions of photoresist film are rendered soluble in the developer (typically an aqueous solution of 0.2−0.3 N tetramethylammonium hydroxide). First used in electronic manufacturing applications in the 1960s, the performance of these materials has been continually improved by careful optimization of the polymer and DNQ dissolution inhibitor. Today, highly optimized DNQ−novolak resists are used to manufacture integrated circuits with device geometries as small as 350 nm.

Unfortunately these resists are not suitable for use at deep-ultraviolet (DUV) wavelengths ($\lambda \approx 250$ nm), the succeeding evolutionary step in the progression of optical lithography tools to higher resolution. There are two principal reasons for this. The first is a consequence of the high absorbance of the DNQ−novolak film at wavelengths below 300 nm. The strong attenuation of the light beam results in a highly nonuniform conversion of the DNQ dissolution inhibitor through the depth of the film. Attempts have been made to modify this chemistry by using more transparent matrix polymers (e.g., poly(hydroxystyrene)) and alternative diazoketone-based dissolution inhibitors,[12] but to date, these modified materials have not met the requirements of high-volume manufacturing. In part, this is due to the complexity of optimizing the dissolution properties of the polymer/dissolution inhibitor pair but also is a consequence of the inherent inefficiency of the photochemical process that leads to resist solubilization. This is a fundamental limitation that has necessitated the development of a new class of photoresists.

The quantum yield for the Wolff rearrangement shown in Figure 5 is ~0.1−0.3.[13] This translates into a required exposure energy of 100−200 mJ/cm^2 for a wafer coated with a typical DNQ−novolak photoresist. At these exposure energies, high wafer throughput (the number of imaged wafers produced per hour per exposure tool) can be readily achieved with the mercury arc lamp sources used throughout the industry. The first DUV resists were developed for use with these same exposure systems, but the mercury lamp output at 254 nm is much weaker than that at longer wavelengths. Contemporary DUV exposure tools are based on KrF excimer sources which are high-intensity sources of light at 248 nm. However, the requirements imposed by the design of the exposure tool projection optics (specifically the introduction of optical line narrowing elements to minimize the effects of chromatic aberration) leads to a significant reduction of the light intensity at the wafer plane. In practice, regardless of the light source, DUV photoresists require approximately a 10× improvement in photoefficiency compared to DNQ-based resists.

One way of achieving this increased efficiency is via the photochemical generation of an initiating species or catalyst that is active in subsequent thermal reactions. A familiar example of the former case is found in photoinitiated free-radical polymerizations and is extensively used in the production of printed circuit boards.[14] A single photochemical reac-

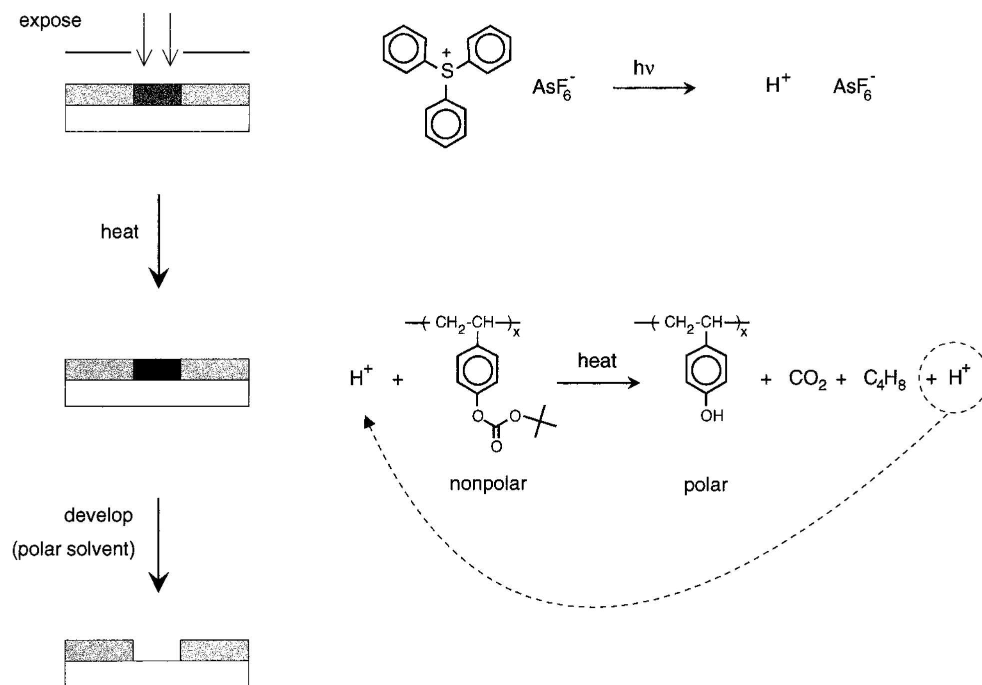

Figure 6. Imaging chemistry for a first-generation chemically amplified DUV resist.

tion (free-radical formation) can result in a large number of subsequent olefin polymerization reactions and an effective quantum yield that is much higher than that of the initiating photochemical reaction and which can exceed unity. Negative-tone photopolymerization resists that rely on this sort of "chemical amplification" (CA) are not suitable for use in microlithographic applications due to their poor resolution.[14]

DUV Chemically Amplified Resists Based on Acid Catalysis. The DUV resists in use today are based on an alternate route to chemical amplification,[15,16] shown schematically in Figure 6. The resist consists of a polymer with an acid-labile pendent group, i.e., poly(*tert*-butoxycarbonyloxystyrene) (PTBOCST), and an onium salt photoacid generator (PAG). In this approach, the photochemical reaction generates a low concentration of a strong Brönsted acid ($HAsF_6$ in the case illustrated). Subsequent thermolysis of the polymer, mediated by the acid catalyst, fragments the pendent *tert*-butoxycarbonyloxy (TBOC) groups. In this fashion, the nonpolar PTBOCST is converted into base-soluble poly(hydroxystyrene), regenerating the acid catalyst while liberating carbon dioxide and isobutylene. The number of TBOC groups cleaved per photogenerated acid molecule has been estimated to be in the range of 1000.[17] As a consequence, this resist, and others based on this CA concept, are much more sensitive than the corresponding DNQ–novolak resists, with imaging doses typically in the 20–30 mJ/cm^2 range. Imaging doses as low as 1 mJ/cm^2 have been reported.[18]

Since the initial demonstration of this concept in the early 1980s, a number of these acid-catalyzed CA resist systems have been developed[19] for manufacturing applications at DUV wavelengths (248 nm and soon to be implemented at 193 nm). Though originally developed nearly 20 years ago to extend the lifetime of a photolithographic exposure tool one more technology generation,[20] CA resists also exhibit high sensitivity when exposed to high-energy radiation such as X-rays and charged-particle beams and, therefore, are considered a key technology that enables future lithographic techniques for imaging in the sub-100 nm range of dimensions.

CA resists differ from DNQ-based resists in a fundamental way. In the latter case, the dissolution inhibitor component (the DNQ) is itself photoactive (Figure 5). In the case of a CA resist such as the TBOCST system, the photolytic conversion of PAG to photogenerated acid does not of itself significantly promote dissolution.[21] The photoactivity and solubilization functions are separate, and reaction of the acid with the protected phenols bound to the polymer backbone is required to realize a significant change in polymer solubility. The efficiency of this conversion will be a function of the kinetics for the deprotection reaction, the postexposure bake temperature and time, acid–base equilibria within the resist film, photoacid volatilization, influence of airborne environmental constituents at the surface of the resist, and the effects of acid diffusion. Each of these factors will influence the performance and resolution of the resist.

The sulfonium salt shown in Figure 6 was one of the first PAG's used in CA resists. Although many types of nonionic PAG's have since been described,[19] onium salts continue to be widely used.[22] These materials have high quantum yields of acid production, good absorption properties at 248 nm, and good solubility and thermal stability in resist films. Onium salts often can be synthesized via metathesis reactions, so it is relatively easy to modify the acid counterion. This affords an easy means to vary the pK_a, volatility, and size of the photogenerated acid. Figure 7 lists a variety of different onium salt and nonionic PAG's.[23]

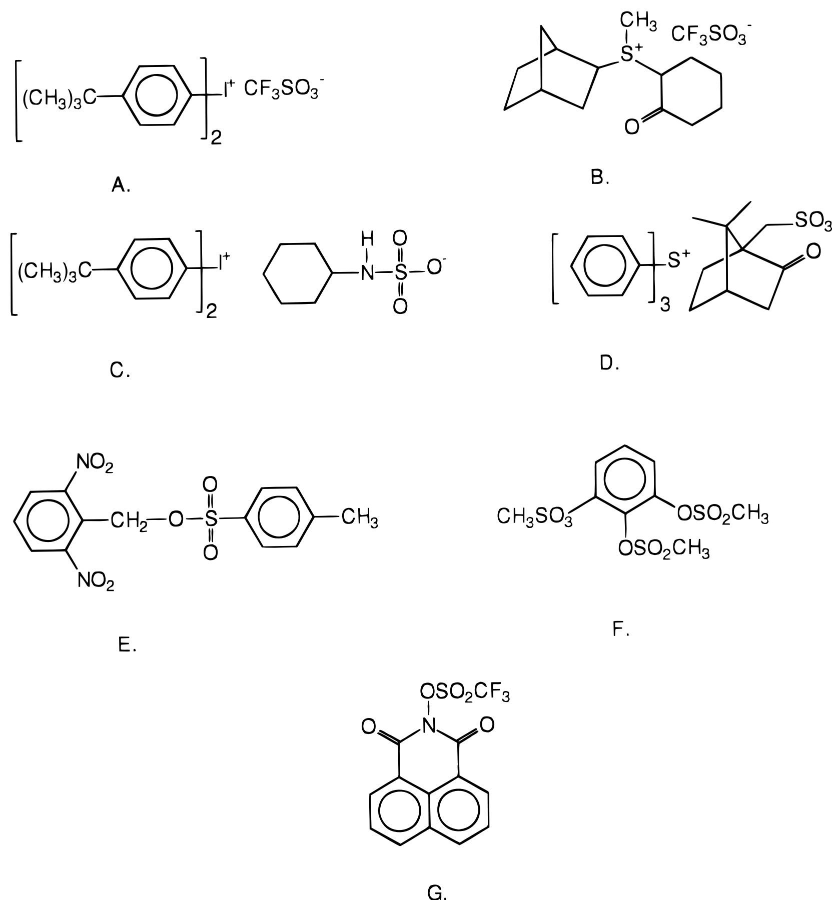

Figure 7. Structures of selected onium salt and nonionic photoacid generators (See ref 23.)

The photochemical pathways leading to acid generation are complex and not fully understood at present. Radical cations have been proposed as the source of acid in both direct irradiation and in electron-transfer sensitized reactions.[24] In the latter case, the absorber can be either the polymer matrix[25] or an added aromatic sensitizer.[26] Proposed mechanisms for both types of reaction are shown in Figure 8.

Most commonly, positive-tone CA resist chemistry is based on the fragmentation of acid-labile ester or carbonate groups or the acid-catalyzed hydrolysis of ketal or acetal functions on the polymer chains. Such reactions are generally thought to proceed via specific acid catalysis.[27] In this mechanism (shown in Scheme 1), the first step is a rapid equilibrium between the photogenerated acid and the acid-labile protecting group. The rate of the reaction is then proportional to the concentration of the protonated protecting group. A typical example of this is the cleavage of *tert*-butyl acetate under strongly acidic conditions.[28]

While this scheme illustrates the basic imaging mechanism, a full description of the chemistry in a reacting CA resist film must include other factors. The photoacid formed on exposure will be in equilibrium with the acid-labile protecting group as well as other film components such as adventitious water, residual casting solvents, and resist additives such as coating aids. In the case of very strong photoacids (e.g., trifluoromethanesulfonic acid), which are completely dissociated under these conditions, the presence of even relatively weak bases can significantly alter the kinetics of deprotection and consequently the imaging behavior of the resist (pK_a's of protonated esters and ethers are in the range from −6 to −7).[29] A graphic example of this can be found in the extreme environmental sensitivities of some of the first DUV CA photoresist systems used in semiconductor manufacturing. Low concentrations (at the ppb level) of organic bases, even weakly basic substances such as *N*-methylpyrrolidone, neutralize the photo acid at the surface of the resist film and inhibit the deprotection reaction required to make the photoresist film soluble.[30] The net result is the formation of an insoluble skin or crust that does not dissolve in the developing solution. This problem can be addressed in a variety of ways, for example, by the use of environmental filtration, by employing resist chemistry that is less affected by contaminants, or by the use of polymers that do not readily absorb these contaminants.[31]

Scheme 1

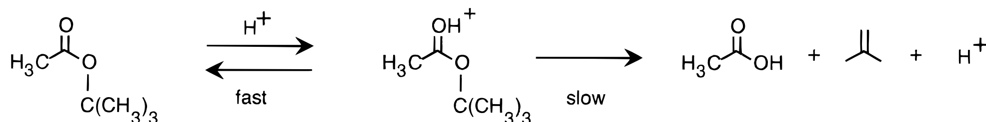

Direct Irradiation

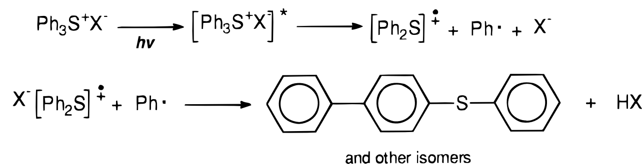

Photosensitization

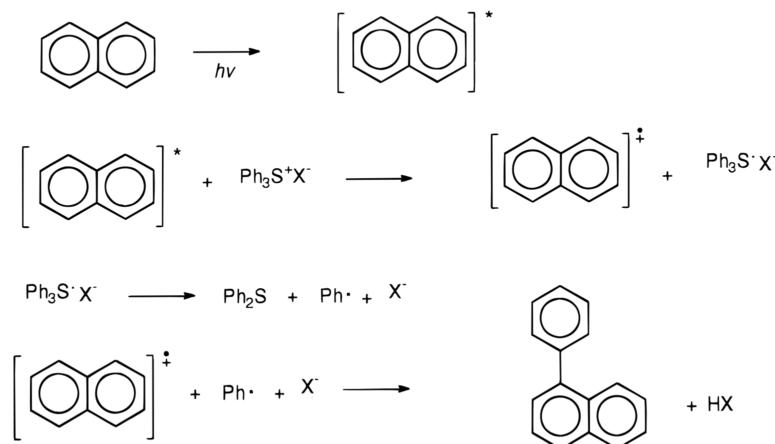

Figure 8. Proposed mechanism for sulfonium salt photoacid generation via both direct photolysis and electron-transfer sensitization.

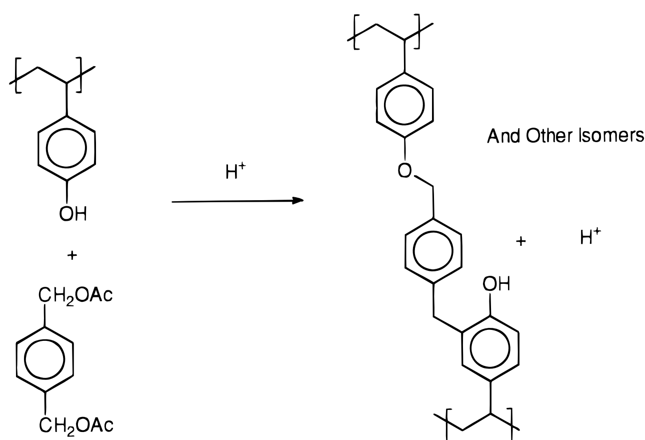

Figure 9. Example of acid-catalyzed cross-linking of a CA negative-tone two-component resist.

Since a spatially nonuniform distribution of acid is formed by the imaging exposure, the kinetics of acid transport within the polymer film also must be considered. The photoacid must diffuse in the exposed regions of the film to effect deprotection. If the acid diffuses into the unexposed areas of the film, however, resolution will obviously suffer. This problem becomes more acute as image dimensions shrink and will be discussed in more detail later.

Until now, our discussion has been confined to a description of positive-tone resists. Acid-catalyzed chemistry can be incorporated into negative-tone photoresists as well.[19] Figure 9 shows an example of the acid-catalyzed reaction of poly(hydroxystyrene) with a monomeric cross-linking agent. True cross-linking is not necessarily required since reaction at a single site may be enough to reduce the solubility of the polymer by an amount sufficient for producing a relief image.

Depending on the actual manufacturing application, the selection of one specific tone of resist may offer an advantage. Positive-tone resists, for example, are particularly well-suited for the printing of "contacts", arrays of closely spaced holes used to electrically connect one layer of the device to another. Negative-tone resists, on the other hand, have attributes which make them well-suited for use in the production of certain of the device shapes encountered in microprocessor fabrication. Figure 10 shows such specific examples of the polymer systems used in both negative- and positive-tone resists. In both of these cases, the goal is to tune the dissolution characteristics of the resist to achieve maximum performance and resolution.

All the polymers shown in Figure 10 are based on the poly(hydroxystyrene) backbone. Recall that high optical absorption was one of the factors that led to the abandonment of novolak resins in favor of poly(hydroxystyrene) for those DUV photoresists designed for 248 nm exposure. As we will discuss later, the same issue appears again in the industry transition from 248 nm exposure tools to higher resolution optical exposure systems designed for exposure with 193 nm emission from an ArF excimer laser. While it is virtually assured that the absorption problem will be successfully circumvented for 193 nm resists, it is less clear that this will be the case when future exposure tools with an even shorter wavelength (e.g., fluorine excimer laser emission at $\lambda = 157$ nm or an extreme-UV (EUV) source using a wavelength of 13 nm) are used. These systems may require a more complex photoresist technology known as thin-film imaging (TFI).[32]

Thin-Film Imaging Resists. Figure 11 shows the process flow for bilayer and top surface imaged (TSI)

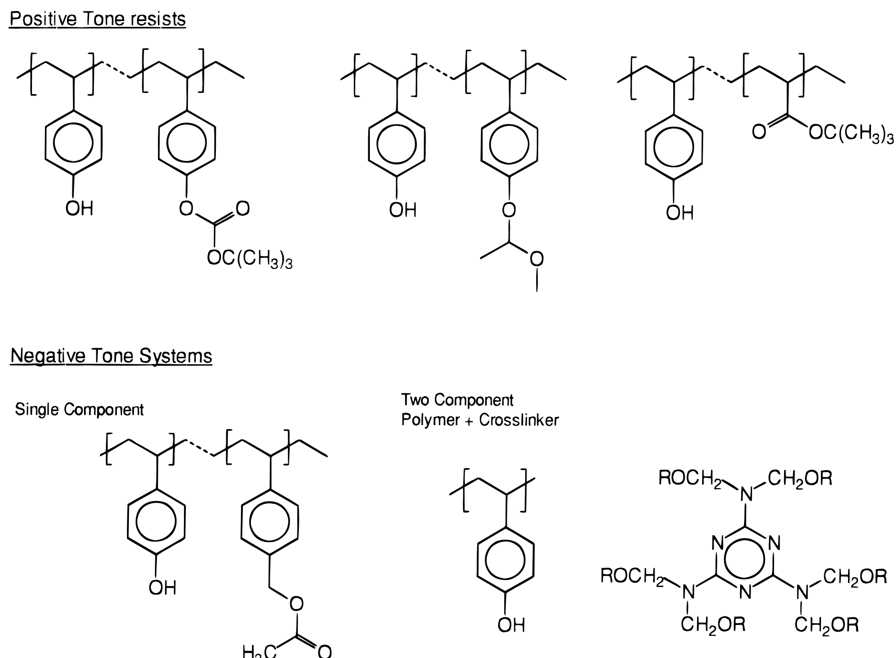

Figure 10. Representative positive- and negative-tone resist systems (see ref 19).

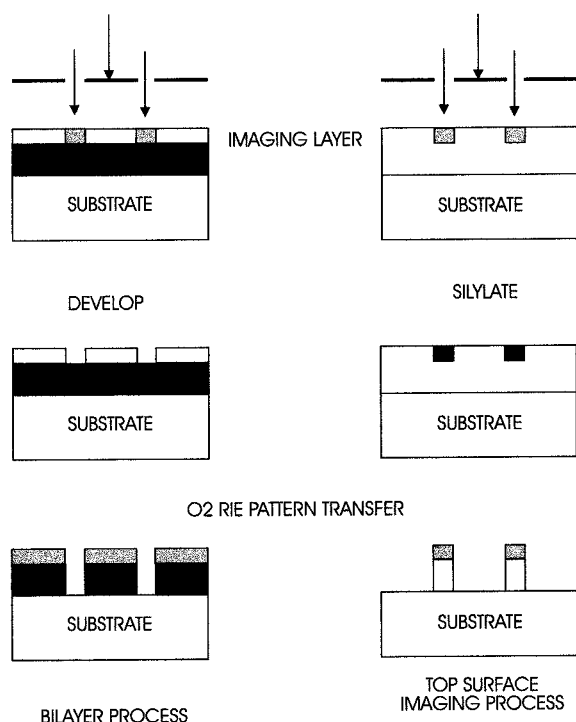

Figure 11. Schematic depicting bilayer and top surface imaging approaches.

resists, the two primary types of TFI systems. In both methods, the imaging layer is thin (100−200 nm thick) and comprises only a fraction of the total resist thickness. After imaging the thin top layer, the resulting image is transferred into a thicker underlayer by an anisotropic etch step using an oxygen plasma. This is possible if the imaging layer contains an element like silicon which forms a refractory oxide under the etch conditions, while the polymer underlayer forms only volatile oxides. When an imaged wafer is placed in an oxygen plasma, the thin patterned layer rapidly forms an etch-resistant film of SiO_2 while the silicon-free underlayer rapidly erodes. By optimization of the etch conditions, this transfer can be done in an anisotropic fashion and the pattern can be transferred vertically into the thicker underlayer. In the case of a bilayer resist, the thin silicon-containing top layer is imaged and developed just like a conventional single-layer resist prior to the oxygen reactive ion etch (O_2−RIE) pattern transfer step.

Another bilayer TFI scheme currently under investigation relies on a very thin imaging layer (on the order of 100 nm) of a conventional resist typically coated on an inorganic film such as silicon oxide which has been deposited on the substrate. After patterning the thin resist layer, the image is transferred to the underlying inorganic film which is employed as a "hardmask" in the subsequent substrate etch. Since the composition of the bilayer is different from that described above (organic imaging layer, silicon-based underlayer), obviously the required etch chemistry will be different (i.e., fluorocarbon-based rather than oxygen-based) for the pattern transfer step. This approach is an attractive candidate for 157 nm and EUV lithography given the high absorbance of current generation photoresists at these wavelengths. Before these so-called "ultrathin resists" (UTR's) can be implemented, practical considerations relating to issues such as defect levels and "pinholes" in thin films will need to be addressed.

TSI resists differ from bilayer systems in that the resist consists of a single film and the silicon that imparts etch resistance is selectively introduced into exposed or unexposed areas of the polymer after the exposure step (Figure 11). By adjusting the opacity of the film, light penetration is confined to the top layer of the resist. If, for example, the PTBOCST resist shown in Figure 6 were imaged at 193 nm, BOC group cleavage would be confined to a depth of only about 100−150 nm due to the high optical density of the film. If this film is then treated with a silylating agent such as dimethylaminodimethylsi-

lane, enough silicon can be incorporated into the exposed regions via reaction with the phenolic hydroxyl groups to provide an etch mask for a subsequent O_2−RIE step. This method should afford very high silylation contrast since there are no reactive sites in the unexposed regions. Cross-linking resists also can be used as TSI resists since diffusion of the silylating agent is retarded in the exposed, cross-linked regions of the film. However, since the entire film is composed of reactive sites in this case, a low level of silylation occurs in the unexposed regions of the film as well. This reduced silylation contrast must be overcome through careful optimization of the etch conditions.

C. Roadmap to Nanometer Sized Devices

Today's most advanced commercial microelectronic devices are manufactured using optical projection lithography at an exposure wavelength of 248 nm employing third-generation chemically amplified DUV photoresists. These devices represent the "250 nm groundrule" generation of integrated circuits, though the smallest dimensions actually printed during the fabrication process are less than that (nearer 200 nm). A typical transistor design contains a gate structure whose dimension strongly influences device speed, and the dimensions of such critical features are reduced to the greatest extent possible while retaining adequate reliability and process control. The upcoming device generation, with 180 nm groundrules, is targeted for commercial availability in 1999. Prototypes are now being fabricated in development and pilot-line settings, again using 248 nm projection exposure tools.

The semiconductor industry has recently charted manufacturing milestones that must be met in the future to maintain the historical rate of technological advancement, where the areal density of function in an integrated circuit increases by a factor of 2 every 3 years. Some of these milestones are indicated in Figure 2. There is consensus that another straightforward evolutionary extension of UV photolithography to shorter wavelength (from 248 nm lithography using KrF excimer laser sources to 193 nm lithography using ArF laser emission) should suffice to manufacture the 130 nm device generation (scheduled commercial availability in 2003). Beyond that, when groundrule dimensions shrink to 100 nm and below, a number of candidate lithography technologies exist, at varying levels of practical demonstration. At present, it is not clear which of these will ultimately find widespread use. The options include extensions of projection lithography to exposure wavelengths of 157 nm (using a F_2 excimer laser source) or 13 nm (using a pulsed laser plasma source), several descendants of the electron-beam method used decades ago to form the structure shown in Figure 1, a related technique using ions rather than electrons, and shadow-printing using X-radiation.

We will explain each of these in more detail, focusing on the physics of latent image formation and the consequences of the physics for the generation of the chemical image. We will then discuss those resist properties that determine ultimate resolution. Finally, we will discuss how the choice of imaging technology dictates the specific requirements for resist properties.

Table 1

	year of product introduction					
	1985	1992	1996	1999	2002	2005
imaging wavelength (nm)	436	365	248	248	193	157
numerical aperture	0.28	0.52	0.6	0.7	0.7	0.7
resolution (nm)	1250	500	250	180	130	100
calculated k_1	0.8	0.7	0.6	0.5	0.47	0.44

IV. Imaging Technologies

A. Next-Generation Optical Lithography

Introduction. Over the past 20 years, the semiconductor industry has succeeded in shrinking device feature sizes 5-fold (from 1.25 μm down to 0.25 μm dimensions) by a combination of decreasing the wavelength of the imaging light and increasing the numerical aperture of the imaging optics (Table 1).[33]

All this has been accomplished without significant change to the nature of the lithographic process. This is indirectly reflected in the value of the k_1 term in the Rayleigh resolution equation (eq 1). Table 1 lists values calculated for k_1. To date, the value of this term has not changed appreciably. Unfortunately, the resolving power of projection optics is approaching a limit (with a practical, maximum NA of no larger than 0.8)[34] and wavelength scaling alone will not be sufficient to achieve the subwavelength resolutions required in the future. The reason for this can be seen from Figure 12, where the aerial image (the light intensity at the surface of the photoresist wafer) for a projection system operating at 248 nm with a numerical aperture of 0.6 is shown.[35] In this example, the mask consists of lines and spaces that are either completely opaque (chrome) or completely transparent (quartz). Under these conditions, this simple binary mask generates a modulated pattern of light with sufficient contrast to resolve 0.25 μm features. Figure 12 also shows the aerial image produced with a similar mask using 193 nm light and a NA of 0.6 for an array of 130 nm lines and spaces. The 130 nm pattern shows much lower image contrast (effectively the intensity ratio between light and dark regions).[36] The aerial image for a 100 nm line/space pattern would show no light modulation at all under these conditions. To resolve features of this size with optical lithography, new illumination schemes, mask technologies, and photoresist processes will be required, all of which will reduce the value of the k_1 term.

Resolution Enhancement. One route for increasing contrast in the aerial image is to modify the mask and/or the illumination system. This is known in the field as applying "resolution enhancement techniques" (RET) or "wavefront engineering".[34] An example of the former is the "biasing" of features on the mask to a size different from the desired final target dimension in order to compensate for limitations in optical and/or resist resolution. This deliberate distortion of mask shapes to compensate for

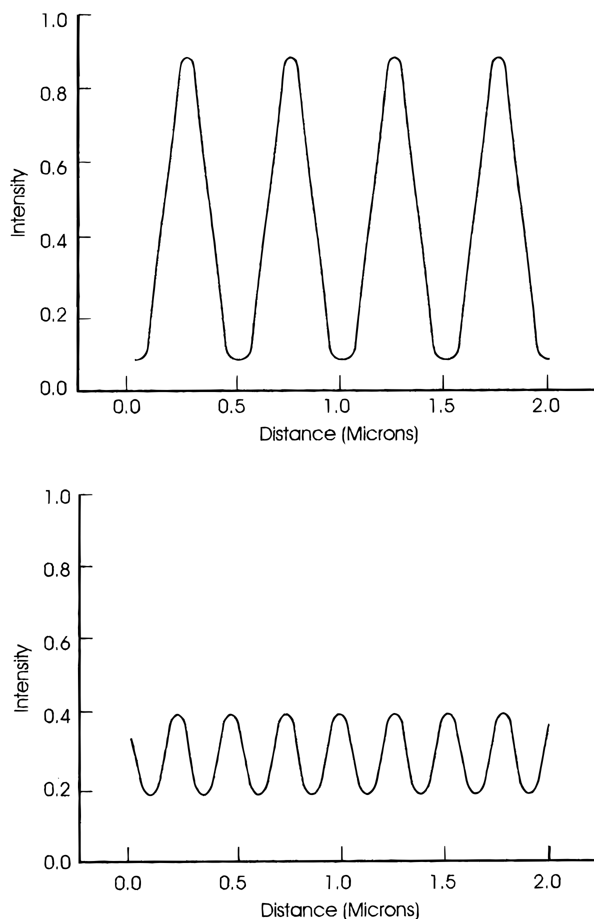

Figure 12. Comparison of image contrast for a 250 nm line/space array (248 nm exposure, 0.6 numerical aperature) (top curve) and a 130 nm line/space array (193 nm exposure, 0.6 numerical aperature) (bottom curve).

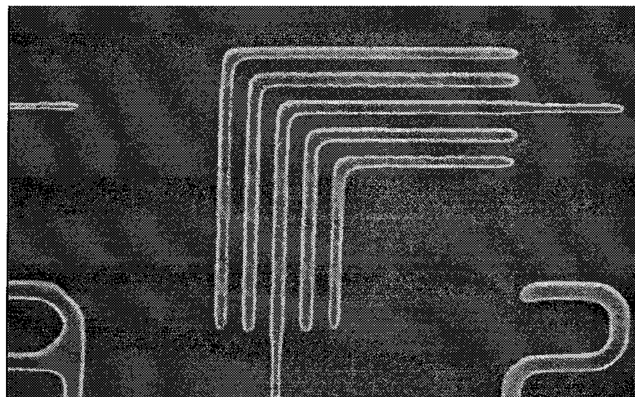

Figure 13. Scanning electron micrograph showing a top-down view of a 200 nm developed resist pattern.

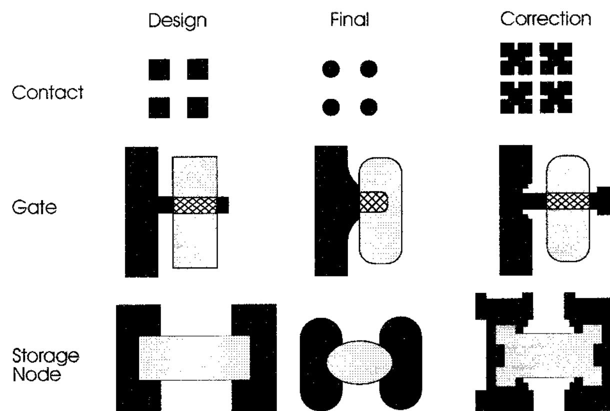

Figure 14. OPC mask shapes for three different device structures. (Photo courtesy L. Liebmann IBM Microelectronics.)

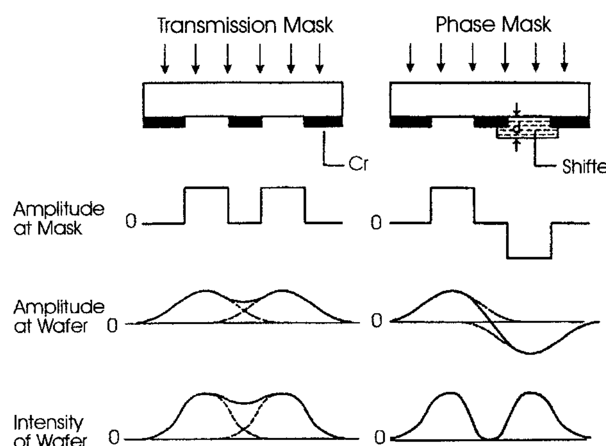

Figure 15. Comparison of conventional binary chrome-on-quartz mask with an alternating aperture phase mask.

systematic patterning inaccuracies is broadly termed optical proximity correction (OPC). It can be used to optimize the aerial image for different types of patterned features. This is necessary because, near a tool's limits of resolution, the light intensity for individual feature elements will be affected by the adjacent pattern. For example, an isolated line would be expected to print differently than a line of the same nominal dimension when it is in the middle of an array of similar sized lines (see an example in Figure 13, though not all of the line slimming in this instance is due to purely optical effects). The problem becomes more acute when irregular arrays are considered, and quite complicated mask features may be required to accurately produce the desired resist image (Figure 14).[37]

Another mask technology provides significantly greater improvements in resolution than OPC. Phase-shift masks differ from conventional binary masks in the way optical interference is employed to improve the quality of the image projected on the wafer. Figure 15 shows, for the case of a simple binary mask, how the light images from adjacent apertures overlap to degrade the aerial image. Since the phase of the electric field from adjacent apertures is identical, constructive interference causes the light intensity between the apertures to be larger than the sum of the individual intensities. In the limit of features that are too small for the optical system to resolve, a transmission mask of this type will produce a uniform level of illumination at the wafer.

If, on the other hand, the phase of the electric field alternates (a 180° phase shift) for adjacent apertures, overlap of the light images will result in destructive interference and the light intensity between the bright spaces will be less than the sum of the contributions from the individual apertures (Figure 15). In this case, interference effects enhance the resolution, with brighter spaces and darker lines.

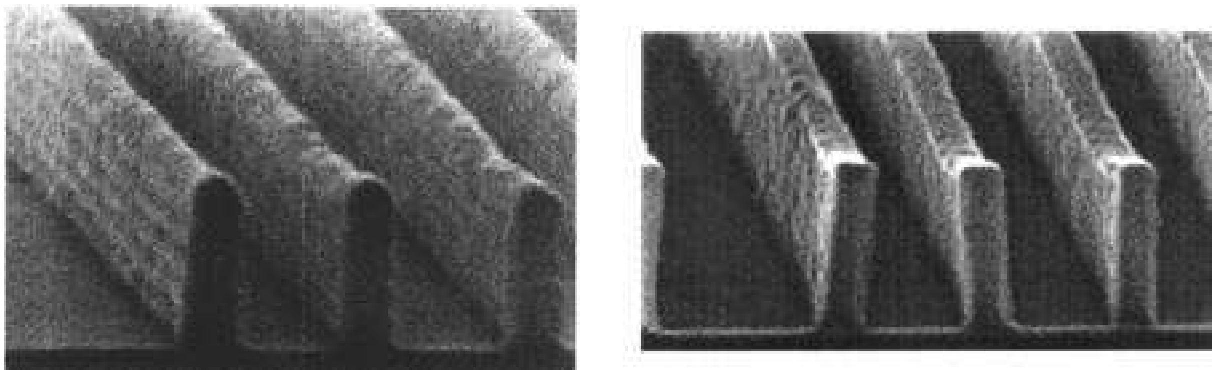

Figure 16. Electron micrographs for 100 nm features printed with 248 nm exposure (left) and 80 nm features printed with 193 nm exposure. (Photos courtesy of J. Petersen, International SEMATECH. Reprinted with permission from SPIE.)

Resolution enhancement of up to 50% is achievable provided the partial coherence of the optical system is adjusted appropriately.[37] For this type of "alternating aperture" phase-shift mask (sometimes referred to as a Levenson–Shibuya mask), the entire image would become dark for features that are too small to be resolved. Figure 15 shows aerial images for line-space arrays for both types of masks.

The 180° phase shift can be introduced by changing the optical path length for alternating adjacent mask features, for example, by adding a phase-shifting element (as shown above) or by etching the mask substrate to a depth sufficient to introduce 1/2 wave of phase shift ($0.5\lambda/(n - 1)$), where n is the refractive index of the substrate. Practical implementation of this type of mask requires the development of methods for the inspection and repair of mask phase defects. While the semiconductor industry has developed techniques for detecting and repairing both transparent and opaque defects in conventional binary masks (i.e., by using excimer laser ablation to remove the residual chrome defects in nominally transparent regions of the mask), there is at this time no clear solution to the identification and repair of phase defects.[34]

There are number of other types of phase-shift masks besides the alternating type just described. An example of a so-called "weak" phase-shifting design is the "leaky-chrome" or "attenuated" mask.[38] In this approach, the opaque chrome found in a conventional mask is replaced by a partially transparent material that also produces a 180° phase shift. Since transmission is only approximately 7%, the resolution enhancement is not as dramatic as with the alternating aperture design. However, the relative ease of fabrication for this mask type makes it a popular approach for resolution enhancement.

Some of the resolution and depth of focus improvements found using phase-shift masks can also be achieved through modifications to the illumination system. Conventional imaging requires that the +1 and −1 diffracted orders be collected by the lens in addition to the undiffracted zeroth order (light that passes directly through the mask). If instead the mask is illuminated in an oblique fashion, only a single diffracted order is required in addition to the undiffracted light to accurately reproduce the mask image. This can be accomplished by illuminating the mask through a pupil fit with four symmetrically disposed openings (quadrupolar illumination) or a partially transparent annulus (annular illumination). The best improvement can be seen for dense line/space gratings; other feature types may exhibit degraded resolution.[39] Off-axis illumination is often combined with attenuated phase masks since the disadvantages of each is offset by the other.

By using a combination of these types of resolution enhancement technologies, researchers have recently reported resolving 100 nm features with a 248 KrF stepper with a relatively low NA (0.53).[40] At 193 nm exposure, even finer features can be produced; Figure 16 shows a line/space array of 80 nm lines printed with an alternating phase mask in an experimental single-layer resist.[41]

Thus far, resolution limitations have been discussed only in terms of the aerial image projected in the resist film. There are, however, other factors that could lead to image degradation. Photoexcited phenolic substituents in 248 nm resists are known to be active in electron-transfer reactions with both onium and nonionic photoacid generators,[42] and while this type of electron exchange photosensitization requires near contact between donor and acceptor (maximum separation of ca. 10−20 Å), prior excitation migration among the phenolic substituents could result in activation of the PAG in what was originally an unexposed region of the film. This type of energy migration can be of the dipole−dipole type that can occur over longer distances (20−40 Å with a maximum of up to a distance of 10 nm for a single hop)[43] and has been documented for a number of aromatic polymers.[44] While this certainly is a consideration in assessing the ultimate resolution capability of optical lithography, there are a couple of things that argue against its importance. Present-generation DUV resists have PAG concentrations on the order of 0.01−0.1 M (with a corresponding average separation between photoactive molecules of 10−30 nm),[45] which should provide efficient quenching of the excited polymer. Long-range excitation transfer is most common in aromatic polymers, and consequently, it is not clear how much of an issue it will be for resists developed for 193 and 157 nm lithography.

Maskless interferometric imaging techniques provide one way to assess the ultimate resolution limits of optical imaging.[46] In this approach, the interference of two coherent light beams is used to generate a sinusoidal standing wave pattern of light intensity

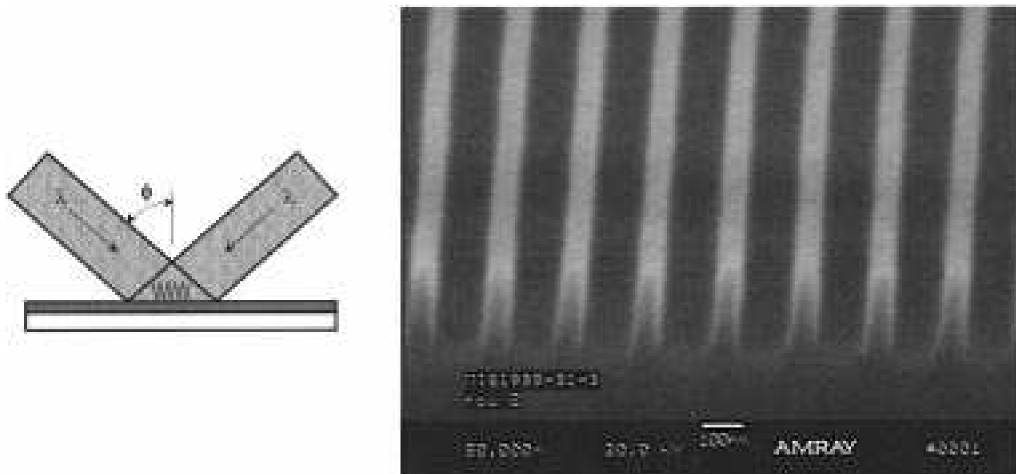

Figure 17. Interferometric lithography: (a) schematic diagram showing the intersecting laser beam configuration, (b) scanning electron micrograph of a resist image printed in a commercial DUV photoresist (Shipley UVIIHS).

in the photoresist film (Figure 17). Line-space arrays can be printed where the period P is determined by the wavelength of light and the angle of intersection of the beams according to the equation

$$P = \lambda/2 \sin \phi \tag{3}$$

where λ is the exposing wavelength and ϕ is the angle of incidence of the beams from the normal. For example, using light beams with a wavelength of 257 nm incident at an angle ϕ of 80°, a line/space array of period 130 nm (65 nm lines/65 nm spaces) is calculated from eq 3, feature sizes roughly one-half that attainable with a state-of-the-art 248 nm projection tool. This method has other advantages as well. The period of the pattern can be varied continuously over a wide range by simple mechanical adjustment of the optical system, the depth of focus is typically very large (from tens of microns to centimeters), and aerial image contrast can be modified by controlling the intensities of the intersecting beams.[47] Using this method, sub-100 nm line-space arrays can readily be printed (Figure 17).

Resists for 193 and 157 nm Exposure. A large proportion of current research in microlithographic materials is devoted to the design of high-resolution single-layer resists suitable for 193 nm exposure using an ArF excimer laser light source.[48] The current focus of this research is the development of resists that do not contain strongly UV-absorbing aromatic chromophores (i.e., hydroxystyrene units) yet which exhibit the low plasma etch rates characteristic of most aromatic systems. The stability of aromatic polymers in an etching plasma has been correlated with their high carbon-to-hydrogen ratio: the higher the percentage of carbon−carbon bonds (i.e., the more "graphitic" the polymer), the more resistant it will be to erosion by the chemical reactions and physical sputtering that can occur during pattern transfer.[49] On the basis of this correlation, a number of acrylic-based polymers with alicyclic functionality pendent to the polymer backbone have been examined for suitable lithographic and plasma etch properties. Such polymers have adequate transparency since the acrylate repeat unit shows only a weak $n-\pi^*$ carbonyl absorption at 193 nm. A wide variety of polymers incorporating acid-labile esters of methacrylic acid can be readily synthesized. The introduction of monomers bearing cyclic side groups such as adamantyl or norbornyl significantly improves the etch resistance over that of simple acrylic polymers. Empirical relationships between the etch rate and structural parameters such as the carbon:hydrogen ratios[50] or number of rings present in the polymer[51] have been described.

Alicyclic structures can be incorporated directly into the polymer backbone. This offers a second route to 193 nm single-layer resists. Metal-catalyzed addition polymerizations, free-radical polymerizations, and ring-opening polymerization techniques[52] have been used to prepare polymers of the type shown in Figure 18. Like the polyacrylic systems, these CA resists implement an imaging mechanism based on the acid-catalyzed deprotection of esters to yield carboxylic acids. Thin films of poly(carboxylic acids) dissolve much more rapidly than films of poly(phenols) in the alkaline developer solutions that have been adopted as industry standards. The rapid dissolution kinetics pose a challenge in designing resists with the correct solubility characteristics;[53] with appropriate selection of comonomers, however, this can be accomplished. The SEM photomicrograph shown in Figure 16 was printed with a resist consisting of the components shown in Figure 18.[41]

Research on exposure systems designed to use the 157 nm output of an F_2 excimer laser as illumination is now in a very early stage.[54] The high optical absorbance of single-layer 248 and 193 nm photoresists at this wavelength will necessitate the design of resists based on alternative polymer systems[54b] or require the use of some form of thin-film imaging such as TSI. Evaluation of a cross-linking poly(hydroxystyrene) TSI resist system developed for 193 nm applications demonstrated that a comparable process window can be achieved using 157 nm exposure.[54] Resist lines 80 nm in width have been printed using this silylated resist and a phase-shift mask fabricated from a calcium fluoride blank.

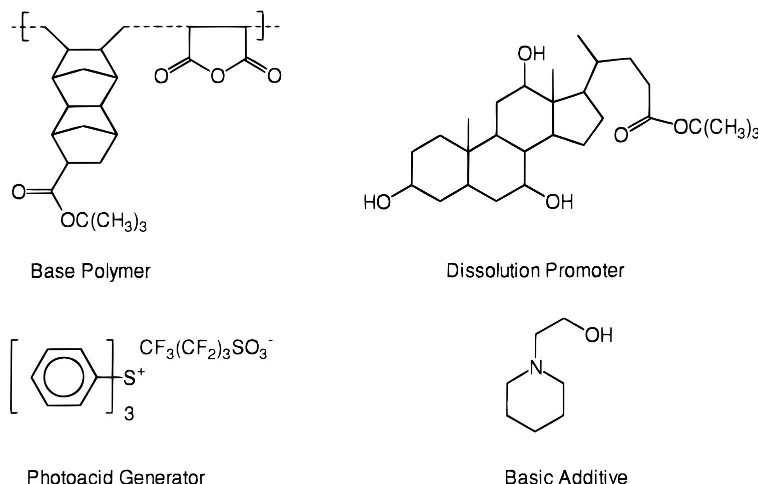

Figure 18. Photoresist components employed in an experimental 193 nm resist. In addition to the etch-resistant cycloaliphatic polymer and the fluoroalkylsulfonic photoacid generator, a cycloaliphatic acid labile dissolution promoter and an amine additive to control acid diffusion have been incorporated into the formulation.

B. Particle Beams

Electron-Beam Lithography. In electron-beam lithography (EBL)[55] a stream of electrons with kinetic energies in the range of 1−100 keV is brought into focus on a resist-coated substrate. Collisions of the electrons with atoms in the resist film create reactive intermediates whose deactivation chemistry changes the properties of the resist film in the irradiated regions. The de Broglie wavelength of electrons in this energy range is extremely small (ca. 8 pm at 25 keV), so that unlike optical lithography, the minimum resolution achievable with EBL tends to be limited by residual aberrations in the electron optics and by electron−electron repulsion at high beam currents that blur the beam (the space−charge effect) rather than by electron diffraction.

Electron−Solid Interactions. The interaction of electron beams with the resist film and the underlying substrate is complex.[56] The fraction of the total beam energy dissipated in the resist depends on the magnitude of the beam energy. As the electron beam passes through the resist, it undergoes small-angle scattering in the forward direction which can cause the beam to be larger in diameter at the resist−substrate interface than at the surface of the resist film. The impinging electrons generate a cascade of secondary electrons with relatively low energy, which in turn cause the formation of free radicals and radical cations. The deactivation of these intermediate species through fragmentation or reaction with the matrix is the basis for the chemical change in the resist film upon exposure.

As the beam passes into the substrate, a significant fraction of the electrons are backscattered into the resist film over an area larger than the desired pattern feature. The exposure chemistry that results from these backscattered electrons is convolved with that from the initial passage of the beam, leading to a complex overall profile of energy deposition in the film. The net outcome is that the total electron dose received by a feature and consequently the shape of the feature depends on the shape of that feature and that of neighboring features and is termed a "proximity effect".

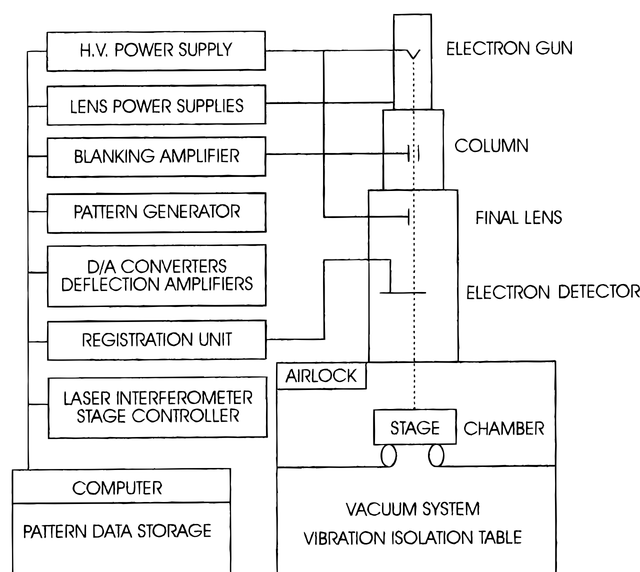

Figure 19. Schematic of a typical electron-beam lithography exposure tool, showing the electron gun, column, and wafer stage.

Electron-Beam Lithography Hardware. A typical direct-write EBL system (Figure 19) employs a single tightly focused electron beam as the radiation source. Electrons produced by a thermionic or field-emission gun are focused by a series of electrostatic or magnetic lenses to a fine spot. The beam current is modulated on and off by a beam-blanking subsystem while the spot is deflected across the surface of the sample. To form the exposed pattern, several writing strategies can be employed: a "vector-scan" approach where the Gaussian beam is deflected from one exposed feature to another, pausing at each to fill in the feature with a series of tightly spaced lines; a "raster-scan" technique where the sample stage moves continuously as the Gaussian beam is deflected back and forth to form the exposed features; and a "shaped spot" method where the beam is formed into one of a set of simple shapes which is used to expose a large-area feature in the resist film in one shot while the beam is stationary. These methods can be considered serial writing techniques,

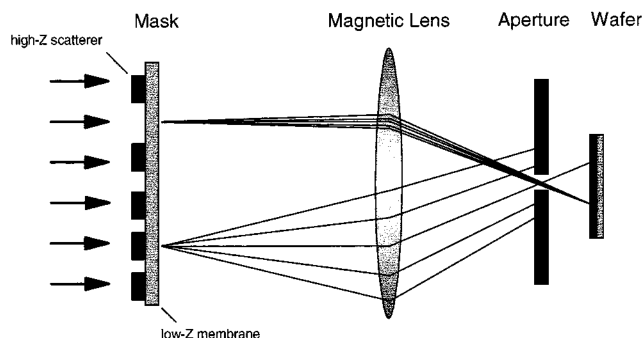

Figure 20. Operating principle of SCALPEL projection electron-beam lithography system.

where the total time to expose a pattern increases linearly with the pattern complexity and chip size. The low productivity compared to optical lithography has limited the commercial use of such EBL tooling to specialized low-volume applications such as the fabrication of optical masks. Several routes to achieving increased throughput by adding parallelism to conventional EBL technology have been proposed. These involve either methods for the formation and control of a number of parallel beams that all simultaneously expose the resist film[57,58] or by the use of micromachining techniques to miniaturize the electron column shown in Figure 19 to only a few millimeters in height.[59] Miniaturization will allow many inexpensive microcolumns to be arranged in an array format for simultaneous exposure.

One approach for improved parallelism in EBL departs from the direct-write, focused-beam approaches we have detailed thus far. In this technique a thin membrane mask transparent to electrons is patterned with a material that strongly scatters electrons (Figure 20).[60] When an electron beam is passed through the scattering mask structure and then focused on a small aperture, the unscattered electrons pass through the aperture while in large part the scattered electrons do not. The net result is the projection of a high-contrast image through the aperture onto a substrate. This method, termed SCALPEL (an acronym for scattering with angular limitation in projection electron-beam lithography) has been demonstrated to have the capability for imaging at feature dimensions at 80 nm.[61] To minimize pattern distortions in the electron optics, only a small (ca 1 mm^2) portion of the mask is illuminated with the electron beam. In SCALPEL the mask and wafer are mechanically scanned through the beam in sychronization to expose the complete pattern. A related technique termed PREVAIL (for projection exposure with variable axis immersion lenses) combines electronic-beam scanning and mechanical scanning to expose the entire circuit pattern.[62]

Electron-Beam Resists. A number of polymeric materials which exhibit little or no sensitivity to UV radiation will undergo efficient degradation when exposed to an electron beam.[63] One of the first polymers recognized to exhibit sensitivity to electron-beam radiation was high molecular weight poly(methyl methacrylate) (PMMA).[64] Electron−solid interactions lead to extensive chain scission of the PMMA chains. The fragmented chains rapidly dissolve in organic developer mixtures to yield positive-tone imaging. Examples of other resist polymers developed specifically for electron-beam lithography and now used commercially include poly(2,2,2-trifluoroethyl-α-chloroacrylate) (sold as EBR-9 by Toray, Inc.), poly(α-chloroacrylate-*co*-α-methylstyrene) (supplied by Nippon Zeon Co as ZEP-520), and poly(butene-1-sulfone). Figure 21 depicts the electron-beam radiation chemistry of poly(butene-1-sulfone).[65,66]

Many resist materials developed for optical lithography can also serve as electron-beam resists. In general, the electron-beam radiation chemistry can differ substantially from the photolytic path, and there is poor correlation between photosensitivity and electron-beam sensitivity.[67]

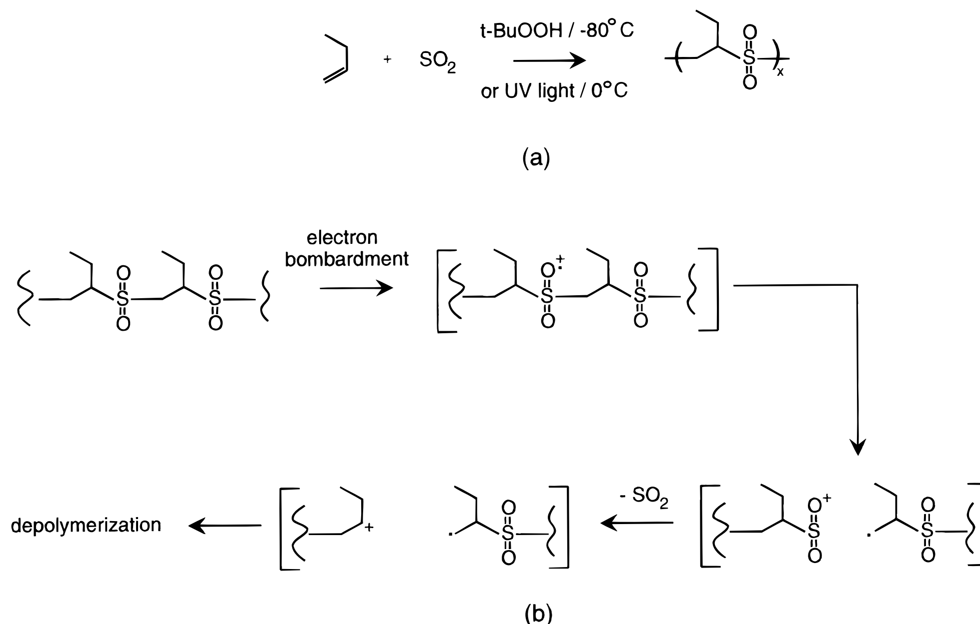

Figure 21. Electron-beam resist chemistry, illustrated for poly(butene-1-sulfone): (a) polymer synthesis, (b) proposed polymer fragmentation pathway.

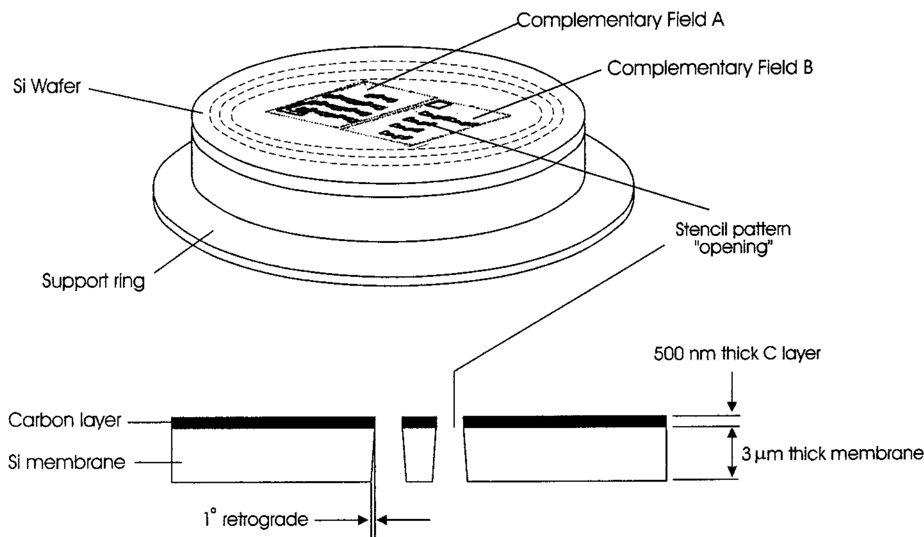

Figure 22. Schematic diagram of a mask for projection ion-beam lithography. (Photo courtesy G. Gomba, IBM.)

Ion-Beam Lithography. The principles of ion-beam lithography (IBL)[56] are closely related to those of EBL. The impinging electron beam is replaced by a beam of accelerated ions, for example, Ga^+, H^+, or He^+. As in EBL, the ions generate low-energy secondary electrons within a resist film, triggering the chemical reactions that lead to lithographic imaging. Therefore, a resist material that exhibits acceptable lithographic properties for EBL (or X-ray lithography—see below) can also be used for IBL. The energy loss from ions in a resist material is much more efficient than the energy loss from electrons,[68] leading to two important consequences for imaging. First, the penetration of the particle beam into the substrate is much less than that with EBL, reducing the image blurring due to scattering that causes a proximity effect. Second, the more efficient energy deposition effectively yields an increased radiation sensitivity for a given resist. While improved sensitivity is desirable in most circumstances, in the IBL case a high-sensitivity resist exposed at the correct dose might require so few ions that statistical fluctuations in the number of ions per pixel leads to poor control of the dimensions of the pattern.

IBL has been implemented in several forms. Focused IBL[69] is analogous to direct-write EBL and shares with it the inherent throughput penalty characteristic of a serial writing process. In masked IBL[70] a collimated ion beam is passed through a thin, ion-transparent membrane patterned with an absorber material and the transmitted beam exposes a resist-coated substrate in proximity to the mask.

There is currently a formal effort to develop a third variant, projection IBL, as a viable candidate for future nanolithographic imaging applications.[71] Conceptually, projection IBL is in many ways analogous to optical projection exposure tools.[72] A divergent ion beam illuminates a mask and is then focused and demagnified by a set of projection ion optics onto a resist-coated substrate. The mask in this case is a stencil, that is, it has physical openings to selectively transmit portions of the ion beam (Figure 22).

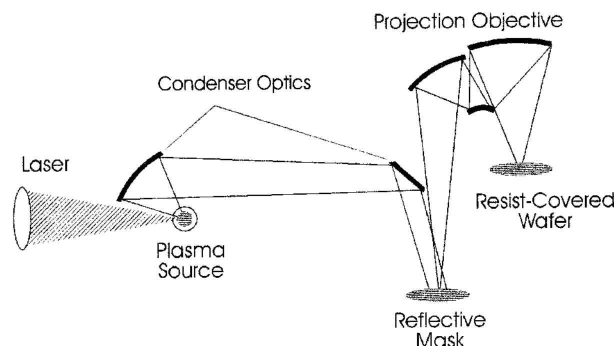

Figure 23. Schematic diagram of an EUV optical system.

C. EUV

Extreme ultraviolet (EUV) lithography (also known as soft X-ray lithography) was first proposed as a candidate for the production of semiconductors with 100 nm features in 1988.[73] It is a form of step-and-scan projection lithography wherein an optical system is used to focus a demagnified image (e.g., a 4× reduction) of the reticle pattern on to the wafer. Figure 23 shows a schematic diagram of an EUV exposure system. This technology can be viewed as an evolutionary extension of the DUV optical imaging techniques described earlier. The principal differences are consequences of the energy range of the exposing light, which is in a wavelength region where essentially all materials are strong absorbers. These very short "UV" wavelengths (13 nm in current generation prototype tools) offer the expected advantages in resolution and DOF (70 nm resolution should be achievable with an NA of 0.1 at a k_1 of 0.5) but require that the optical system be operated in high vacuum and preclude the use of transmissive and refractive optical components.

Synchrotrons, free-electron lasers, and hot plasmas can serve as sources of EUV radiation, but the latter is preferred for lithography applications.[74] A hot plasma can be generated during the irradiation of a solid target with a high-power pulsed laser. The laser heats the material, stripping electrons from ablated atoms to create a plasma. Subsequent heating of this plasma by the laser pulses results in excitation to

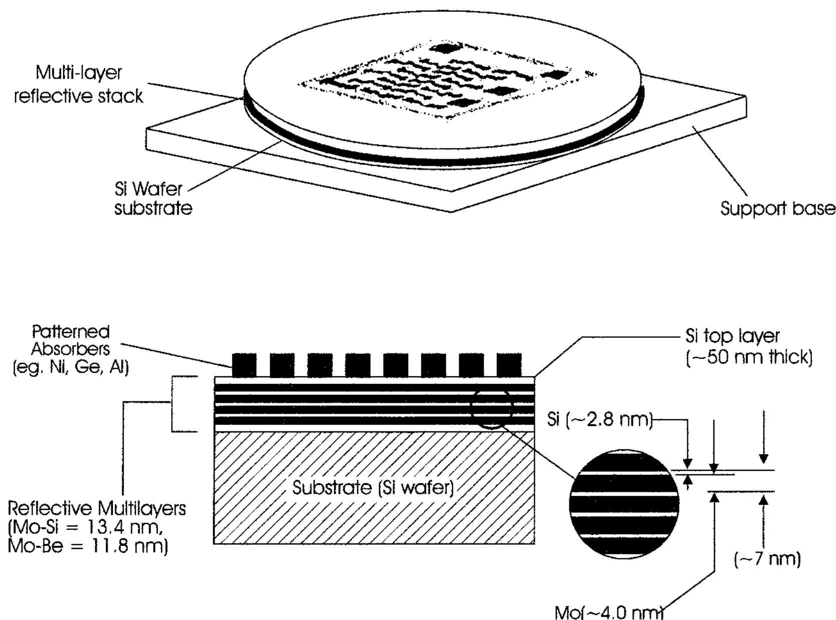

Figure 24. Schematic diagram for an EUV reflective mask. Cutout shows multilayer film stack required to maximize reflectivity. (Photo courtesy G. Gomba, IBM.)

the higher ionization states that produce X-ray emission. Efficient generation of EUV light requires a laser pulse energy of 0.5−1 J over a duration of 5−10 ns, at an intensity at the target of $\sim 3.0 \times 10^{11}$ W/cm^2.[75] The conversion efficiency of laser light to EUV light is approximately 2% or less under these conditions. Ablation of target material can also introduce significant amounts of debris which can deposit on the condenser optics and damage the exposure system. There are a variety of approaches being investigated to eliminate this problem, including the use of supersonic gas jets.[76]

Perhaps the biggest challenge for EUV lithography is the fabrication of X-ray optical components, all of which must be reflective. Mirrors are fabricated from multilayer dielectrics (for example, alternating layers of molybdenum and silicon) coated on curved and flat optical surfaces. They are analogous to the dielectric mirrors used for visible and ultraviolet optics, but, while a mirror designed to operate at 193 nm can reflect up to 99% of the incident radiation, the best EUV mirrors currently have reflectivities of only 60−70% at 13 nm. This low reflectivity limits the number of reflective surfaces permitted in the exposure system and consequently places constraints on the design of the condenser and imaging optics. Moreover, these optical components must be fabricated at extremely high tolerances with mirror surface errors of less than 1 nm and require the development of optical metrology tools capable of this level of accuracy.[77]

EUVL masks also must be reflective and are fabricated using the same multilayer dielectric coatings employed in mirror fabrication. The mask consists of a patterned metal absorber sitting atop a multilayer reflective coating, deposited on an opaque substrate such as silicon (Figure 24). The absorber is patterned using conventional EBL. Since any defect generated during the fabrication of the multilayer mask blank (which can consist of up to 40 layer pairs of Mo−Si) cannot be repaired in the completed mask, ultraclean deposition techniques are required.[78]

Aerial image formation in EUV lithography is similar to that already described for optical imaging. At 13 nm the range of photoelectrons is quite low (less than 5 nm), so unlike proximity X-ray and e-beam lithography, the effect of secondary electrons on the resolution is negligible. Absorption of X-rays is dependent on the atomic weight percent and the density of the elements in the absorbing film, and can be calculated from the mass absorption coefficients of the individual elements.[79] Phenolic- and acrylate-based resists absorb strongly at this wavelength. As a consequence, both top-surface imaging[80] and bilayer TFI schemes are being investigated. It is anticipated that high resist sensitivities will be required ($\sim$ 5 mJ/cm^2), so it is likely that chemically amplified resists will be necessary.

D. Proximity X-ray

The first demonstration of X-ray lithography was reported in the early 1970s.[81] Since that time a great deal of research has gone into developing this technology for semiconductor manufacturing.[82] It is based on shadow or proximity printing, where the mask is separated from the wafer by a small gap (typically less than 100 μm). No focusing optics are employed, so a 1× mask is required, with feature sizes identical to those to be printed on the wafer.

For lithographic applications, X-radiation can be generated by either a point-source hot plasma (as in the case of EUV lithography) or a synchrotron source. In the latter, X-rays are emitted as a highly collimated beam from relativistic electrons that are constrained to travel in a circular or elliptical orbit. Compact storage rings, specialized synchrotrons that are small enough and inexpensive enough to be suitable for lithographic applications, consist of a

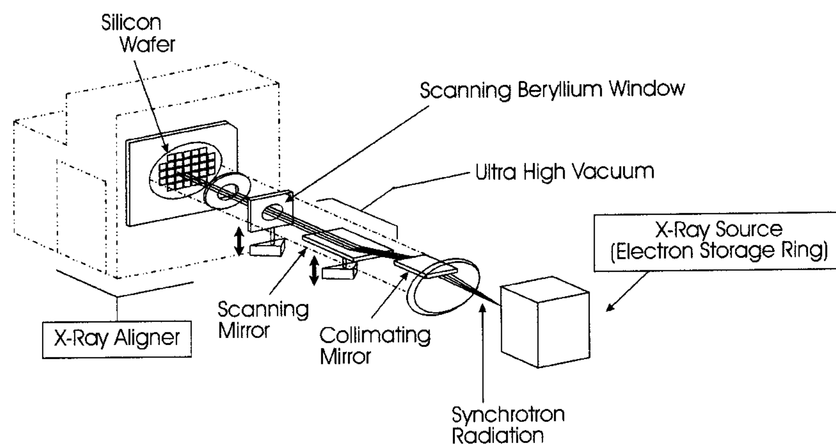

Figure 25. Schematic diagram of a proximity X-ray exposure system.

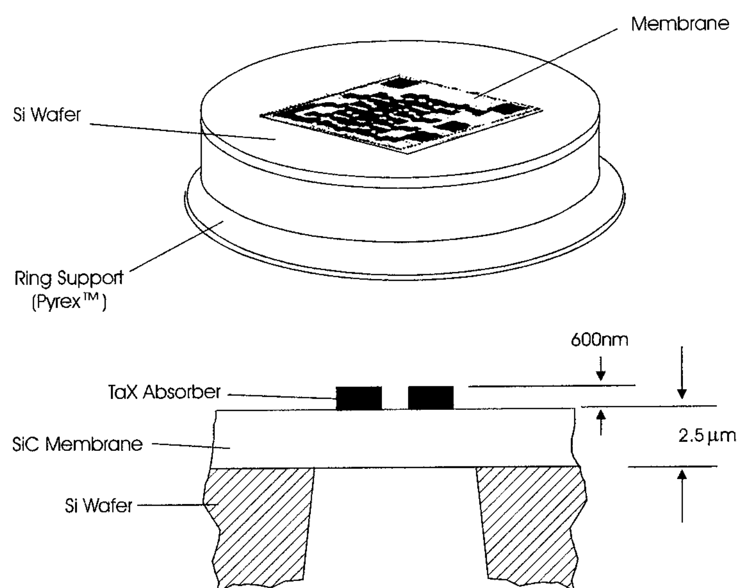

Figure 26. Schematic diagram of a 1× proximity X-ray mask. (Photo courtesy G. Gomba, IBM.)

source of high-energy electrons as well as RF acceleration cavities which maintain the ring at constant energy levels, thereby compensating for the energy lost as emitted X-radiation. Power output for such a system is on the order of 100 mW/cm^2, significantly higher than that of a point source. In consequence, storage rings are the system of choice for semiconductor manufacturing. A single storage ring can serve as the source for multiple steppers (Figure 25).

The optimal wavelength range for X-ray lithography is dependent on resist sensitivity,[83] mask transparency,[84] and diffraction effects[85] and is usually regarded to be between 0.8 and 1.4 nm.[86] At wavelengths this short, even the all-reflective optical systems used in EUV are not practical, hence proximity printing is the only alternative. Whereas resolution in optical lithography is defined in terms of wavelength and the NA of the projection optics (Fraunhofer diffraction), in X-ray imaging the critical parameters are wavelength and the spacing between mask and wafer (Fresnel diffraction). The Fresnel number

$$f = w^2/\lambda g \quad (4)$$

(where w = feature size, λ = wavelength, and g = the distance between mask and wafer) is similar to the k_1 value in the optical lithography equation (eq 1). An f value of 1 would be required to print 100 nm features at 1 nm wavelength with a 10 μm mask to wafer gap. At separations this small, avoiding inadvertent contact between mask and wafer places stringent requirements on wafers and mask flatness, mechanical control of the mask position in the stepper, and control of particulates on the wafer. As with the k_1 term in optical lithography, smaller values of f can be achieved through the use of resolution-enhancement methods.

A diagram of an X-ray mask is shown in Figure 26. It consists of a thin, X-ray transparent (typically silicon carbide) membrane approximately 1 μm thick, patterned with a high atomic number absorber such as tungsten or tantalum at a thickness of 0.3−0.5 μm. The mask substrate should be thin to maximize X-ray transmission at the wavelengths required for resist exposure. A relatively thin absorber layer is dictated in part by the difficulties of fabricating thick, high-aspect-ratio features (the height/width ratio) and the need to minimize stress-distortion of the mask membrane. Since the thin absorber layer does not absorb

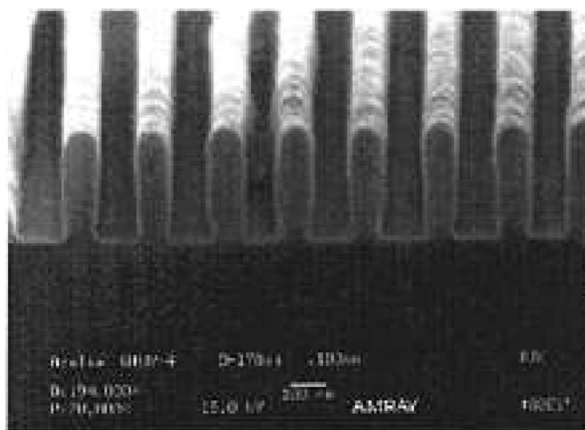

Figure 27. Scanning electron micrograph of 100 nm grating printed in a DUV photoresist. (Photo courtesy of A. Krasnoperova, IBM Microelectronics.)

all the X-radiation, the contrast of X-ray masks is poor compared to optical masks with opaque chrome patterns. These "leaky" absorbers can serve as phase-shifting elements, and in fact the advantages of phase shifting were recognized for X-ray imaging before the technique was applied to optical lithography.[87] The fabrication of defect- and distortion-free masks for sub-100 nm lithography places severe demands on current generation EBL mask writing tools.[82]

There are two factors limiting the resolution of X-ray lithography: photoelectron "blur" and diffraction. X-rays absorbed by the resist produce photo- and Auger electrons. In the case of 0.8 nm photons, this amounts to a maximum photoelectron range of 40–70 nm in poly(methyl methacrylate).[88] Resist resolution, however, is determined not by the total range of electrons but by the spatial distribution of deposited energy. The region where the energy density is high enough to render the polymer soluble is much narrower than the total range, consistent with early demonstrations of 30 nm features printed in this polymer.[89] Diffraction-limited resolution for X-ray lithography is dependent on the mask to wafer gap as shown in eq 4. As feature sizes drop to 70 nm and below, gaps of less than 10 μm are likely to be required along with tuned and optimized mask structures.[90]

The large penetration depth and the absence of interfacial reflections enable the use of single-layer X-ray resists. A variety of CA- and DNQ-based resists can be used for X-ray applications.[82] Figure 27 shows 100 nm resist features printed in a 248 nm CA resist with a mask gap of 10 μm. Note that this is a 1:1 line-space array; printing this type of grating structure is significantly more challenging than printing isolated or semi-isolated lines. Imaging in this case was done with an exposure dose of 170 mJ/cm^2.[91] Resist sensitivities of less than 50 mJ/cm^2 are desired to improve throughput.[92]

V. High-Resolution Resists

In all of the lithographic techniques discussed so far, a chemical latent image is generated that is subsequently developed by wet or dry processes to form the final relief pattern in the resist film. In CA resists this latent image of deprotected or cross-linked functional groups is formed by conversion of the initial photoacid profile generated by the imaging exposure. Blurring of this profile as a consequence of acid diffusion leads to degradation of the chemical latent image before development. Other resolution-limiting factors also can occur during both wet and dry development. In the following sections we will describe these effects in more detail.

A. Latent Image Formation

The photogenerated acid in CA resist films must be free to diffuse in order to catalyze the imaging chemistry. For example, in Scheme 1, rate constants for the protonation of the acid-labile resist components in the equilibration step are dependent on the acid diffusion coefficients. In the case of a strong acid reacting with a strong base, the reaction is diffusion limited.[93] In solution, where typical diffusion coefficients are on the order of 10^{-5} cm^2/s, such a reaction has a bimolecular rate constant of ca. 10^{10} mol^{-1} s^{-1}. Diffusion coefficients of small molecules in glassy polymers below T_g are significantly slower; typical values are on the order of 10^{-10} cm^2/s (10^{-2} μm^2/s), so one expects smaller protonation rate constants and slower overall reaction rates compared to those in solution. As a consequence, a complete understanding of resist reactivity requires a knowledge of acid diffusion as well as resist kinetics.

While acid migration within the exposed areas of the film is necessary, excessive diffusion into unexposed areas of the film will lead to a loss of image fidelity. In fact, when CA resists were first proposed it was believed by some that this type of diffusion would seriously limit their use for high-resolution applications. Although subsequent experiments demonstrated resolution well below 100 nm for the TBOCST system,[94] for many other CA resists the control of acid diffusion remains a critical issue.

There are several techniques that have been applied to moderate diffusion. Since mobility in glassy polymers is a function of the molecular size of the diffusant, the use of photoacid generators that produce bulky photoacids (for example, camphorsulfonic acid) has been proposed as a means to reduce acid diffusion lengths.[95]

Another method employs basic additives to quench the acid if it diffuses out of the exposed area of the film.[96] The base also neutralizes the acid in the exposed regions, so this direct additive approach is accompanied by a net loss in resist radiation sensitivity. In a variant of this technique intended to circumvent the sensitivity loss, the added base is photoactive. Photogeneration of acid takes place simultaneously with photodegradation of the base in exposed areas. This minimizes the sensitivity loss of the added base but still leaves base in the unexposed areas where it can effectively neutralize migrating acid.[97]

Since acid diffusion in polymers is a thermally activated process, decreased postexposure bake temperatures will reduce the extent of diffusion. At low temperatures, however, the deprotection kinetics of TBOCST and *tert*-butyl ester carboxylate systems

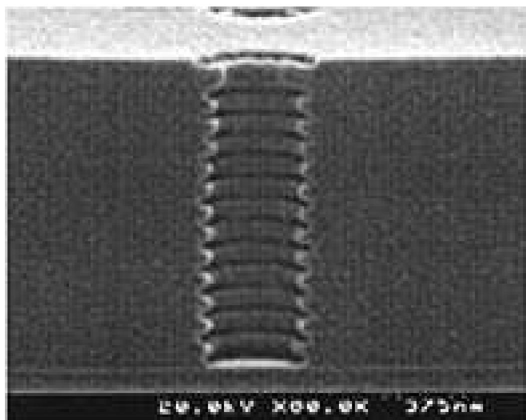

Figure 28. Sidewall notching in a DUV photoresist, a consequence of standing wave formation during imaging on a reflective substrate.

become unacceptably slow, so in this case the imaging chemistry must be based on low E_a reactions, such as the hydrolysis of acetal or ketals.[98]

While excessive diffusion is generally the concern, it is possible to have insufficient diffusion under certain conditions. Figure 28 shows a scanning electron micrograph of a developed contact hole in a DUV resist exposed at 248 nm on a reflective substrate. The sidewall notching pattern is a consequence of light intensity variations within the film. Interference between the reflected and incoming light generates the standing wave light intensity pattern and consequently concentration gradients of the photogenerated acid. Similar effects are well-known in nonchemically amplified DNQ resists where the notching can be removed by baking the wafer prior to development.[99] As a consequence of the coupling of diffusion and deprotection chemistry in CA resists, this simple solution for the removal of standing waves is not necessarily applicable in these systems.

As acid diffuses through the resist film, the polymer matrix concurrently undergoes reaction. In a positive-tone resist, the acid-catalyzed cleavage reactions can change the polarity of the film, generate volatile byproducts, and cause film shrinkage. Similar changes can occur in negative-tone photoresists, accompanied by the formation of a cross-linked network. As a result, acid diffusion in CA resists is quite complex and considerably more complicated than the diffusion of inert small molecules in polymer matrices.[47]

A number of reports have described methods for the characterization of acid diffusion in resist polymers. In many of these, the extent of acid diffusion is inferred from measurements of the developed resist profiles, i.e., by measuring line width change as a function of resist formulation and processing conditions.[100] Interpretation of these data is complicated by the fact that the developed resist profile is a convolution of the initial latent image of acid, the resist chemistry, acid diffusion, and the nonlinear resist dissolution properties. Experiments intended to quantify photoacid diffusion by ion conductivity measurements,[101] correlations with acid volatilization,[102] absorption of acid vapor[103], STM measurements,[104] and recently laser confocal microscopy[105] have been described. In another approach, acid transport between two contacted polymer films is measured. Here, only one film contains the acidic species while the other contains acid-labile groups which serve as a detection mechanism for transported acid.[106] In recognition of the role that acid diffusion plays in CA resist lithographic process, there has been a significant effort at incorporating acid diffusion parameters into lithography modeling software.[107]

Many of the reported diffusion coefficients range between 1×10^{-4} and 1×10^{-6} $\mu m^2/s$, significantly slower than the typical values for diffusion of small molecules in glassy polymers cited above. A diffusion coefficient of 3.0×10^{-6} $\mu m^2/s$ (measured in a DUV 248 nm resist by ion conductivity) translates into a diffusion length of 23 nm under the processing conditions employed in the study.[108] While this represents only 10% of the line width for the current devices (250 nm). it is equal to one-third of the line width at the 70 nm generation. While a great deal of effort has gone into trying to understand the impact of acid diffusion in CA resists, as feature sizes continue to shrink, further study will be required.

B. Line-Edge Roughness

Random fluctuations in the width of a resist feature have been termed line-edge roughness (LER). It has been recognized for some time that the amplitude of LER can be a significant fraction of the overall resist feature width at small feature dimensions and in such cases poses a difficulty in dimensional control.[109] Since the resist LER can be replicated or even increased in the final device structure by the image-transfer process, LER is expected to become a factor in device performance at sub-100 nm critical dimensions. A study of LER in TSI resists has established a correlation between LER and surface roughness of exposed, silylated, and developed TSI resists.[110] This result was interpreted as stemming from statistical effects in this intermediate region that lead to spatially nonuniform silicon incorporation at the nanoscale. This result leads to the prediction that LER in TSI resists is linked to aerial image contrast, and TSI imaging results are consistent with this prediction.[110]

LER has been observed in a variety of single-layer resists as well. Evidence has been presented that the molecular weight distribution of the resist polymer and the molecular structure of resist components can influence the magnitude of LER in negative-tone electron-beam resists.[111,112] Interferometric lithography has been used to demonstrate that LER in single-layer CA resists is also influenced by aerial image contrast, analogous to the effect demonstrated in the TSI resist process.[47] The spatially inhomogeneous solubility properties that lead to LER in this case may be due to nonuniform dispersion of the photoacid generator in the film,[113] nanoscale statistical variations in the extent of acid-catalyzed deprotection,[114] or statistical effects on the solubility of polymer chains.[115]

VI. Summary

Historically, microlithographic technology has followed an evolutionary path where incremental improvements in techniques, materials, and tooling have enabled progress at a rapid rate. In this review we have recounted the reasons why such evolutionary advancement is not likely to suffice for future lithographic imaging at sub-100 nm dimensions. We have described the characteristics of alternate resist and imaging technologies now under development which the industry has termed next-generation lithographies for the sub-100 nm era.

While the forces that drive the semiconductor industry virtually ensure that large-scale manufacturing of sub-100 nm devices will take place at some point in the future, it is impossible to predict, at present, which of the candidate technologies will find application there. Both technical and economic considerations play key roles in this decision. Research in the exposure and resist technologies described in this review continue at a swift pace, and a review of the field 5 years from now may be radically different from the current work.

VII. References

(1) Ajayan P. M. *Chem. Rev*. **1999**, *99*, 1787.
(2) Bosman, A. W.; Janssen, H. M.; Meijer, E. W. *Chem. Rev.* **1999**, *99*, 1665.
(3) Chen, C. C.; Herhold, A. B.; Johnson, C. S.; Alivasatos, A. P. *Science* **1997**, *276*, 398.
(4) Avouris, P. *Acc. Chem. Res*. **1995**, *28*, 95.
(5) Broers, A. In *First International Conference on Electron and Ion Beam Science and Technology*; Bakish, R., Ed.; Wiley and Sons: New York, 1964; p 191.
(6) *1997 National Technology Roadmap for Semiconductors*; The Semiconductor Industry Association: San Jose CA, 1997.
(7) Whitesides, G. *Chem. Rev*. **1999**, *99*, 1823.
(8) Hartsuch, P. *Chemistry of Lithography*; Lithographic Technical Foundation: New York, 1961.
(9) Holmes, S.; Mitchell, P.; Hakey, M. *IBM J. Res. Dev.* **1997**, *41*, 7.
(10) Born, M.; Wolf, E. *Principles of Optics*, 6th ed.; Pergamon Press: Oxford, 1983; pp 415, 441.
(11) (a) Dammel, R. *Diazonaphthoquinone-based Resists*; Tutorial Texts in Optical Engineering, v. TT 11; SPIE Optical Engineering Press: Bellingham, WA, 1993. (b) Willson, C. G. *Introduction to Microlithography*, 2nd ed.; ACS Professional Reference book; Americian Chemical Society, Washington, DC, 1994; Chapter 3. (c) Reiser, A. *Photoreactive Polymers*, *The Science and Technology of Resists*; Wiley-Interscience: New York, 1989; Chapter 5.
(12) Leeson, M. J.; Pawloski, A.; Levering, V.; Willson, C. G. *Proc. SPIE* **1997**, *3049*, 871.
(13) Dammel, R. *Diazonaphthoquinone-based Resists*; Tutorial Texts in Optical Engineering, v. TT 11; SPIE Optical Engineering Press: Bellingham, WA, **1993**; p 15.
(14) Moreau, W. M. *Semiconductor Lithography: Principles*, *Practices*, *and Materials*; Plenum Press: New York, 1988; p 199.
(15) Ito, H.; Willson, C. G. *Polym. Eng. Sci*. **1982**, *23*, 1021.
(16) Frechet, J.; Ito, H.; Willson, C. G. *Proc. Microcircuit. Eng.* **1982**, *82*, 260.
(17) McKean, D.; Schaedili, U.; MacDonald, S. In *Polymers in Microlithography*; ACS Symposium Series 412; Reichmanis, E., MacDonald, S., Iwayanagi, T., Eds.; Americian Chemical Society: Washington, DC, 1989; p 27.
(18) Ito, H.; Maekawa, Y. In *Polymeric Materials for Microelectronic Applications*; ACS Symposium Series 529; Ito, H., Tagawa, S., Horie K., Eds.; Americian Chemical Society: Washington, DC, 1994; p 70.
(19) Reichmanis, E.; Houlihan, F.; Nalamasu, O.; Neehan, T. *Chem. Mater*. **1991**, *3*, 394.
(20) Willson, C. G.; Dammel, R. R.; Reiser, A. *Proc. SPIE* **1997**, *3049*, 28.
(21) See, however: Ito, H. *Proc. SPIE* **1992**, *1672*, 94.
(22) For a recent review on onium salts, see: Crivillo, J. In *Radiation Curing in Polymer Science and Technology*: *Photoinitiating Systems*; Fouassier, J. P., Rabek, J. F., Eds.; Elsevier: New York, 1993; Vol. II, Chapter 8.
(23) (a) Allen, R.; Wallraff, G.; Hinsberg, W.; Simpson, L.; Kunz, R. In *Polymers for Microelectronics*; ACS Symposium Series 537; Thompson, L. F.. Willson, C. G., Tagawa, S., Eds.; American Chemical Society: Washington, DC, 1994; Chapter 11. (b) Nakano, K.; Maeda, K.; Iwasa, S.; Hasegawa, E. *Proc. SPIE* **1995**, *2438*, 433. (c) Houlihan, F. M.; Kometani, J. M.; Timko, A. G.; Hutton, R. S.; Gabor, A.; Medina, A.; Biafore, J.; Slater, S. *Proc. SPIE* **1998**, *3333*, 73. (d) Cronin, M. F.; Adams, M.; Fedynyshyn, T.; Georger, J.; Mori, J. M.; Sinta, R.; Thackery, J. W. *Proc. SPIE* **1994**, *2195*, 214. (e) Neenan, T.; Houlihan, F.; Reichmanis, E.; Kometani, J.; Bachman, B.; Thompson, L. *Macromolecules* **1990**, *23*, 145. (f) Hayashi, N.; Schlegel, L.; Ueno, T.; Shiraishi, H.; Iwaayanagi, T. *Proc. SPIE* **1991**, *1466*, 377. (g) Ito, H.; Breyta, G.; Hofer, D.; Fischer, T.; Prime, B. *Proc. SPIE*. **1995**, *2438*, 53.
(24) Hacker, N. In *Radiation Curing in Polymer Science and Technology*: *Photoinitiating Systems*; Fouassier, J. P., Rabek, J. F., Eds.; Elsevier: New York, 1993; Vol II, Chapter 9.
(25) Schlegel, L.; Ueno, T.; Shiraishi, H.; Iwayanagi, T. *Chem. Mater*. **1990**, *2*, 299.
(26) Devoe, R.; Sahyun, M.; Schmidt, E. *Can. J. Chem*, **1988**, *66*, 319.
(27) Lowery, T. H.; Richardson, K. S. *Mechanism and Theory in Organic Chemistry*, 3rd ed.; Harper and Row: New York, 1987; Chapter 7.
(28) March, J. *Advanced Organic Chemistry*, 4th ed.; Wiley-Interscience: New York, 1992; p 380.
(29) March, J. *Advanced Organic Chemistry*, 4th ed.; Wiley-Interscience: New York, 1992; p 250.
(30) Hinsberg, W.; MacDonald, S.; Clecak, N.; Snyder, C.; Ito, H. *Proc. SPIE* **1993**, *1925*, 43.
(31) Ito, H. *J. Photopolym. Sci. Technol.* **1998**, *11*, 379.
(32) Miller, R. D.; Wallraff, G. M. *Adv. Mater. Opt. Electron.* **1994**, *4*, 95.
(33) Levinson, H. J.; Arnold, W. H. In *Handbook of Microlithography*, *Micromachining*, *and Microfabrication*; Rai-Choudhury, P., Ed.; SPIE Optical Engineering Press: Bellingham, WA, 1997; Vol. 1, Chapter 1.
(34) (a) Levenson, M. D. *Phys. Today* **1993**, 28. (b) Levenson, M. D. *Solid State Technol.* **1995**, *38*, 57.
(35) For a review of optical lithography modeling, see: Neureuther, A.; Mack, C. In *Handbook of Microlithography*, *Micromachining*, *and Microfabrication*; Rai-Choudhury, P., Ed.; SPIE Optical Engineering Press: Bellingham, WA, 1997; Vol. 1, Chapter 7. Simulations were performed using the SAMPLE program (available from UC Berkeley, Department of Electrical Engineering).
(36) Bowden, M. J. *Introduction to Microlithography*, 2nd ed.; ACS Professional Reference book; American Chemical Society: Washington, DC, 1994; Chapter 2.
(37) Levenson, M. D. *Jpn. J. App. Phys.* **1994**, *33*, 6765.
(38) Lin, J. B. *Solid State Technol.* **1992**, *35*, 43.
(39) Shiraishi, N.; Hirukawa, Y.; Takeuchi, Magome, N. *Proc SPIE* **1992**, *1674*, 741.
(40) Petersen, J. S.; Socha R. J.; Naderi, A.; Baker, C.; Rizvi, S.; VanDenBroeke, D.; Kachwala, N.; Chen, N.; Laidig, T.; Wampler, K. E.; Caldwell, R.; Takeuchi, S.; Yamada, Y.; Senoh, T.; McCallum, M. *Proc. SPIE* **1998**, *3412*, 503.
(41) Patterson, K.; Okoroanyanwu, T.; Shimokawa, T.; Cho, S.; Beyers, J. D.; Willson, C. G. *Proc. SPIE* **1998**, *3333*, 425.
(42) Schlegel, L.; Ueno, T.; Shiraishi, H.; Iwayanagi, T. *Chem. Mater*. **1990**, *2*, 299. Hacker; N. P.; Welsh, K. M. *Macromolecules* **1991**, *24*, 2137.
(43) Gilbert, A.; Baggott, J. *Essentials of Molecular Photochemistry*; CRC Press: Boca Raton, FL, 1991; p 168.
(44) Guillet, J. In *Polymer Photophysics and Photochemistry*; Cambridge University Press: Cambridge, UK, 1985; Chapter 9. Webber, S. E. *Chem. Rev*. **1990**, *90*, 1469.
(45) Turro, N. J. In *Modern Molecular Photochemistry*; Benjamin/Cummings: Menlo Park, CA, 1978; p 319.
(46) (a) Bozler, C.; Harris, C.; Rabe, S.; Rathman, D.; Hollis M.; Smith, H. *J. Vac. Sci. Technol. B* **1994**, *12*, 629. (b) Zaidi S.; Brueck, S. *J. Vac. Sci. Techn. B*, **1993**, *11*, 658. (c) Savas, T.; Shah, S.; Schattenburg, M.; Carter J.; Smith, H. *J. Vac. Sci. Technol. B* **1995**, *13*, 2732. (d) Fernandez, A.; Nguyen, H.; Britten, J.; Boyd, R.; Perry, M.; Kania, D.; Hawryluk, A. *J. Vac. Sci. Technol. B* **1997**, *15*, 729. (e) Brueck, S.; Zaidi, S.; Xhen, X.; Zhang, Z. *Microelectron. Eng.* **1998**, *41–42*, 145.
(47) Hinsberg, W.; Houle, F. A.; Hoffnagle, J.; Sanchez, M.; Wallraff, G.; Morrison M.; Frank, S. *J. Vac. Sci. Technol. B* **1998**, *16*, 3689.
(48) Allen, R. D.; Wallraff, G. M.; Hofer, D. C.; Kunz, R. R. *IBM J. Res. Dev.* **1997**, *41*, 95.
(49) Allen, R. D.; Conley, W. E.; Kunz, R. R. In *Handbook of Microlithography*, *Micromachining*, *and Microfabrication*; Rai-Choudhury, P., Ed.; SPIE Optical Engineering Press: Bellingham, WA, 1997; Vol. 1, Chapter 4.
(50) Gokhan, H.; Esho, S.; Ohnishi, Y. *J. Electrochem. Soc*. **1983**, *130*, 143.

(51) Kunz, R. R.; Palmateer, S.; Forte, A.; Allen, R. D.; Wallraff, G. M.; DiPietro, R.; Hofer, D, *Proc. SPIE* **1996**, *2724*, 365.
(52) Okoroanyanwu, U.; Shimokawa, T.; Beyers, J.; Medeiros, D.; Willson, C. G.; Quingshang, J.; Frechet, J. M.; Allen, R. D. *Proc. SPIE* **1997**, *3049*, 92.
(53) Szmanda, C. R.; Yu, J.; Barclay, G.; Cameron, J.; Kavanagh, R. J.; Blacksmith, R.; Trefonas, P.; Taylor, G. N. *Proc. SPIE* **1997**, *3049*, 65.
(54) (a) Bloomstein, T. M.; Horn, M. W.; Rothschild, M.; Kunz, R. R.; Palmacci, S. T.; Goodman, R. B. *J. Vac. Sci. Technol. B* **1997**, *15*, 2112. (b) Bloomstein, T. M.; Rothschild, M.; Kunz, R. R.; Hardy, D. E.; Goodman, R. B.; Palmacci, S. T. *J. Vac. Sci. Technol. B* **1998**, *16*, 3154.
(55) McCord, M.; Rooks, M. In *Handbook of Microlithography, Micromachining and Microfabrication* Rai-Choudhury, P., Ed.; SPIE Press: Bellingham, WA, 1997; Vol. 1, Chapter 2.
(56) Broers, A. In *Materials for Microlithography*; ACS Symposium Series 266; Thompson, L., Willson, G., Frechet, J., Eds.; American Chemical Society: Washington, DC, 1984; Chapter 2.
(57) Hofmann, W.; Chen, L.; MacDonald, N. *J. Vac. Sci. Technol. B* **1995**, *13*, 2701.
(58) Shimazu, N.; Saito, K.; Fujinami, M. *Jpn. J. Appl. Phys.* **1995**, *34*, 6689.
(59) Kratschmer, E.; Kim, H.; Thompson, M.; Lee, K.; Rishton, S.; Yu M.; Chang, T. *J. Vac. Sci. Technol. B* **1995**, *13*, 2498.
(60) Berger, S.; Gibson, *J. Appl. Phys. Lett.* **1990**, *57*, 153.
(61) Harriot, L. *J. Vac. Sci. Technol. B* **1997**, *15*, 2130.
(62) Pfieffer, H. *Jpn. J. Appl. Phys.* **1995**, *34*, 6658.
(63) Bowden, M. In *Materials for Microlithography*; ACS Symposium Series 266; Thompson, L., Willson, G., Frechet, J., Eds.; American Chemical Society: Washington, DC, 1984; Chapter 3.
(64) Hatzakis, M. *J. Electrochem. Soc*. **1969**, *116*, 1033.
(65) Bowden, M.; Thompson, L. *J. Appl. Polym, Sci.* **1973**, *17*, 3211.
(66) Thompson, L.; Bowdon, M. *J. Electrochem Soc.* **1973**, *120*, 1722.
(67) Rau, N.; Neureuther, A.; Ogawa, T.; Kubena, R.; Stratton, F.; Fields, C.; Willson, G. *Proc. SPIE* **1998**, *3333*, 1413. Nagahara, S.; Kozawa, T.; Yamamoto, Y.; Tagawa. S. *J. Photopolym. Sci. Technol.* **1998**, *11*, 577.
(68) Brunger, W.; Buchmann, L.; Torkler M.; Finkelstein, *W. J. Vac. Sci. Technol. B* **1994**, *12*, 3547.
(69) Seliger, R.; Kubena, R.; Olney, R.; Ward J.; Wang, V. *J. Vac. Sci. Technol.* **1979**, *16*, 1610.
(70) Bartelt, J.; Slayman, C.; Wood, J.; Chen, J.; McKenna, C.; Minning, C.; Coakley, J.; Holman R.; Perrygo, C. *J. Vac. Sci. Technol.* **1981**, *19*, 1166.
(71) Gross, G. *J. Vac. Sci. Technol. B* **1997**, *15*, 2136.
(72) Stengl, G.; Loschner, H.; Maurer W.; Wolf, P. *J. Vac. Sci. Technol. B* **1986**, *4*, 194.
(73) Hawryluk, A. M.; Seppala, L. G. *J. Vac. Sci. Technol. B* **1988**, *6*, 2162.
(74) (a) Hawryluk, A. M.; Ceglio, N. M.; Markle, D. A. *Solid State Technol.* **1997**, 155. (b) Kinoshita, H.; Watanabe, T. *J. Photopolym. Sci. Technol.* **1997**, *10*, 369. (c) See also: Gwyn, C. W.; Stulen, R.; Sweeney, D.; Attwood, D. *J. Vac. Sci. Technol. B* **1998**, *16*, 31212.
(75) Hawryluk, A. M.; Ceglio, N. M.; Markle, D. A. *Solid State Technol.* **1997**, 75.
(76) Kubiak, G. N.; Krenz, K. D.; Berger, K. W. *OSA Proceedings on EUVL* **1994**, *23*, 248.
(77) Tejnil, E.; Goldberg, K. A.; Lee, S.; Medecki, H.; Batson, P. J.; Denham, P.; MacDowell, A.; Bokor, J.; Attwood, D. *J. Vac. Sci. Technol. B* **1997**, *15*, 2455.
(78) Kearney, P. A.; Moore, C. E.; Tan, S. I.; Vernon, S. P.; Levesque, R. A. *J. Vac. Sci. Technol. B* **1997**, *15*, 2452.
(79) Bowden, M. J. In *Introduction to Microlithography*, 2nd ed.; ACS Professional Reference book; Americian Chemical Society: Washington, DC, 1994; Chapter 2. Henke, B. L.; Gullikson, E. M.; Davis, J. C. *At. Data Nucl. Data Tables* **1993**, *54*, 181.
(80) Wheeler, D.; Hutton, R.; Boyce, C.; Stein, S.; Cirelli, R.; Taylor, G. *Proc. SPIE* **1995**, *2438*, 762. Rao, V.; Hutchinson, J.; Holl, S.; Langston, J.; Henderson, C.; Wheeler, D. R.; Cardinale, G.; O'Connell, D.; Goldsmith, J.; Bohland, J.; Taylor, G.; Sinta, R. *J. Vac. Sci. Technol. B* **1998**, *16*, 3722. Henderson, C. C.; Wheeler, D.; Pollagi, T.; Cardinale, G.; O'Connell, D.; Fisher, A.; Rao, V.; Goldsmith, J. *J. Photopolym. Sci. Technol.* **1998**, *11*, 459.
(81) Smith, H. I.; Spears, D. L.; Bernaacki, S. E. *J. Vac. Sci. Technol. B* **1993**, *10*, 913.
(82) Silverman, J. P. *J. Vac. Sci. Technol. B* **1997**, *15*, 2117.
(83) Hector, S.; Pol, V.; Krasnoperova, A.; Maldonado, J.; Flamholtz, A.; Heald, D.; Stahlhammer, C.; Galburt, D.; Amodeo, R.; Donohue, T.; Wind, S.; Buchigniano, J.; Viswanathan, R.; Khan, M.; Bollepalli, S.; Cerina, F. *J. Vac. Sci. Technol. B* **1997**, *15*, 2517.
(84) Cerina, F. In *Handbook of Microlithography*, *Micromachining, and Microfabrication*; Rai-Choudhury, P., Ed.; SPIE Optical Engineering Press: Bellingham, WA, 1997; Vol. 1, Chapter 3.
(85) Smith, H. I.; Schatteburg, M. L. *IBM J. Res. Dev*. **1993**, *37*, 319.
(86) Cerrina, F. *Proc IEEE* **1997**, *84*, 644.
(87) Levenson, M. D. *Proc. SPIE* **1997**, *3049*, 2. Khan, M.; Bollepalli, S.; Cerina, F. *J. Vac. Sci. Technol. B* **1997**, *15*, 2255.
(88) Ocola, L. E.; Cerina, F. *J. Vac. Sci. Technol. B* **1993**, *11*, 2839.
(89) Early, K.; Schattenburg, M. L.; Smith, H. I. *Microelectron. Eng.* **1990**, *11*, 317.
(90) Simon, G.; Harhiri-Gosnet, A. M.; Bourneix, J.; Decanini, D.; Chen, Y.; Rousseaux, F.; Launois, H.; Vidal, B. *J. Vac. Sci. Technol. B* **1997**, *15*, 2489.
(91) Krasnoperova, A.; Hector, S.; Pomerane, A.; Lamberti, A.; Wind, S.; Viswanathan, R.; Ito, H. *J. Photopolym. Sci. Technol.* **1997**, *10*, 613.
(92) Nagaha, S.; Kozawa, T.; Yamamoto, Y.; Tagawa, S. *J. Photopolym. Sci. Technol.* **1998**, *11*, 577.
(93) Hibbert, F. *Advances in Physical Organic Chemistry*; Academic Press: London, 1986; Vol. 22, 113.
(94) Umbach, A. N.; Broers, R.; Koch, R.; Willson, C. G.; Laibowitz, R. B. *IBM J. Res. Dev.* **1988**, *32*, 454.
(95) Cronin, M. F.; Adams, M.; Fedynyshyn, T.; Georger, J.; Mori, J. M.; Sinta, R.; Thackery, J. W. *Proc. SPIE* **1994**, *2195*, 214.
(96) Asakawa, K.; Ushirogouchi, T.; Nakase, M. *Proc SPIE* **1995**, *2438*, 563.
(97) Funato, S.; Kawaski, N.; Kinoshita, Y.; Masuda, S.; Osazaki, H.; Padmanaban, M.; Yammato, T.; Pawlowski, G. *Proc. SPIE* **1996**, *2724*, 186.
(98) Huang, W. S.; Kwong, R.; Katnani, A.; Khojasteh, M. *Proc. SPIE* **1994**, *2195*, 37. Schacht, H. T.; Muenzrl, N.; Falcigno, P.; Holzwarth, H.; Schneider, J. *J. Photopolym. Sci. Technol.* **1996**, *9*, 445.
(99) Dammel, R. *Diazonaphthoquinone-based Resists*; Tutorial Texts in Optical Engineering, v. TT 11; SPIE Optical Engineering Press: Bellingham, WA, 1993; Chapter 2.
(100) (a) Schlegel, L.; Ueno, T.; Hayashi, N.; Iwayanagi, T. *J. Vac. Sci. Technol. B* **1991**, *9*, 278. (b) Yoshiyuki, T.; Nakayama, Y.; Okazaki, S. *J. Vac. Sci. Technol. B* **1992**, *10*, 2615. (c) Cronin, M. F.; Adams, M.; Fedynyshyn, T.; Georger, J.; Mori, J. M.; Sinta, R.; Thackery, J. W. *Proc. SPIE* **1994**, *2195*, 214. (d) Itani, T.; Yoshino, H.; Fujimoto, M.; Kasama, K. *J. Vac. Sci. Technol. B* **1995**, *13*, 3026. (e) Connolly, J.; Chen, K. R.; Kwong, R.; Lawson, M.; Linehan, L.; Moreau, W. *Proc. SPIE* **1998**, *3333*, 1124 (f) Rau, N.; Neureuther, A.; Ogawa, T.; Kubena, R.; Stratton, F.; Fields, C.; Willson, G. *Proc. SPIE* **1998**, *3333*, 1413.
(101) (a)Nakamura, J.; Ban, H.; Deguchi, K.; Tanaka, A. *Jpn. J. Appl. Phys*. **1991**, *10*, 6065. (b) Fedynyshyn, T. H.; Thackeray, J. W.; Georger, J. H.; Denison, M. D. *J. Vac. Sci. Technol. B* **1994**, *12*, 3888.
(102) Thackaray, J. W.; Denision, M. D.; Fedynyshyun, T. H.; Kang, D.; Sinta, R. In *Microlectronics Technology*, *Polymers for Advanced Imaging and Packaging*; ACS Symposium Series 614; Reichmanis, E., Ober, C., MacDonald, S., Iwayanagi, T., Nishikubo, T., Eds.; American Chemical Society: Washington, DC, 1995; p 84.
(103) Mueller, K. E.; Koros, W. J.; Mack, C. A.; Willson, C. G. *Proc. SPIE* **1997**, *3049*, 706.
(104) Perkins, F. K.; Dobisz, E. A.; Marrian, C. R. K. *J. Vac. Sci. Technol. B* **1993**, *11*, 2597.
(105) Zhang, P. L.; Webber, S.; Mendenhall, J.; Beyers, J.; Chao, K. *Proc. SPIE* **1998**, *3333*, 794.
(106) (a) Asakawa, K.; Ushirogouchi, T.; Nakase, M. *Proc SPIE* **1995**, *2438*, 563. (b) Uchino, S.; Yamamoto, J.; Migitaka, S.; Kojima, K.; Hashimoto, M.; Murai, F.; Shiraishi, H. *J. Photopolym. Sci. Technol.* **1998**, *11*, 555. (c) Sakamizu, T.; Arai, T.; Yamaguchi, H.; Shiraishi, H. *Proc SPIE* **1997**, *3049*, 448.
(107) (a) Zuniga, M.; Neureuther, A. R. *J. Vac. Sci. Technol. B* **1995**, *13*, 2957. (b) Petersen, J. S.; Mack, C. A.; Sturtevant J.; Byers, J. D.; Miller, D. A. *Proc. SPIE* **1995**, *2438*, 167. (c) Krasnoperova, A. A.; Khan, M.; Rhyner, S.; Taylor, J. W.; Zhu, Y.; Cerrina, F. *J. Vac. Sci. Technol. B* **1994**, *12*, 3900. (d) Petersen, J. S.; Byers, J. D. *Proc. SPIE* **1996**, *2724*, 164.
(108) Itani, T.; Yoshino, H.; Hashimoto, S.; Yamana, M.; Samoto, N.; Kasama, K. *J. Vac. Sci. Technol. B* **1997**, *15*, 2541.
(109) Yoshimura, T.; Yamamoto, J.; Shiraishi, H.; Uchino, S.; Terasawa, T.; Murai F.; Okazaki, *S. J. Photopolym. Sci. Technol*. **1997**, *10*, 629.
(110) Palmateer, S.; Cann, S.; Curtin, J.; Doron, S.; Eriksen, A.; Forte, A.; Kunz, R.; Lyszczarz, T.; Stern, M.; Nelson, C. *Proc. SPIE* **1998**, *3333*, 634.
(111) Yoshimura, T.; Shiaishis, H.; Yamamoto J.; Okazaki, S. *Jpn. J. Appl. Phys*. **1993**, *32*, 6065.
(112) Yamamoto, J.; Uchino, S.; Hattori, T.; Yoshimura, T.; Murai, F. *Jpn. J. Appl. Phys.* **1996**, *35*, 6511.
(113) McKean, D.; Allen, R.; Kasai, P.; Schaedeli, U.; MacDonald, S. *Proc. SPIE* **1992**, *1672*, 94.
(114) Ushirogouchi, T.; Asakawa, K.; Nakase, M.; Hongu, A. *Proc. SPIE* **1995**, *2438*, 609.
(115) Tsiartis, P.; Henderson, C.; Flanagin, L.; Hinsberg, W.; Sanchez, I.; Bonnecaze, R.; Willson, G. *Macromolecules* **1997**, *30*, 4656.

CR980003I